Tellus (2001), 53B, 646–672
Printed in UK. All rights reserved

Copyright © Munksgaard, 2001
TELLUS
ISSN 0280–6509

# Vertical distributions of sulfur species simulated by large scale atmospheric models in COSAM: Comparison with observations

By U. LOHMANN[1]*, W. R. LEAITCH[2], L. BARRIE[3], K. LAW[4], Y. YI[2], D. BERGMANN[5], C. BRIDGEMAN[4], M. CHIN[6], J. CHRISTENSEN[7], R. EASTER[3], J. FEICHTER[8], A. JEUKEN[9], E. KJELLSTRÖM[10], D. KOCH[11], C. LAND[8], P. RASCH[12] and G.-J. ROELOFS[13], [1]*Atmospheric Science Program, Department of Physics, Dalhousie University, Halifax, NS, B3H 3J5 Canada;* [2]*Meteorological Service of Canada, Downsview, ON, Canada;* [3]*Pacific Northwest National Laboratory, Richland, WA, USA;* [4]*Department of Chemistry, University of Cambridge, UK;* [5]*Atmospheric Science Division, Lawrence Livermore National Laboratory, CA, USA;* [6]*NASA Goddard Space Flight Center, Greenbelt, MD, USA;* [7]*National Environmental Research Institute, Roskilde, Denmark;* [8]*Max Planck Institute for Meteorology, Hamburg, Germany;* [9]*Royal Netherlands Meteorological Institute (KNMI), De Bilt, The Netherlands;* [10]*Stockholm University, Stockholm, Sweden;* [11]*NASA/GISS, New York, NY, USA;* [12]*National Center for Atmospheric Research (NCAR), Boulder, CO, USA;* [13]*Institute for Marine and Atmospheric Research, Utrecht (IMAU), Utrecht University, Utrecht, The Netherlands*

(Manuscript received 1 September 1999; in final form 12 March 2001)

ABSTRACT

A comparison of large-scale models simulating atmospheric sulfate aerosols (COSAM) was conducted to increase our understanding of global distributions of sulfate aerosols and precursors. Earlier model comparisons focused on wet deposition measurements and sulfate aerosol concentrations in source regions at the surface. They found that different models simulated the observed sulfate surface concentrations mostly within a factor of two, but that the simulated column burdens and vertical profiles were very different amongst different models. In the COSAM exercise, one aspect is the comparison of sulfate aerosol and precursor gases above the surface. Vertical profiles of $SO_2$, $SO_4^{2-}$, oxidants and cloud properties were measured by aircraft during the North Atlantic Regional Experiment (NARE) experiment in August/September 1993 off the coast of Nova Scotia and during the Second Eulerian Model Evaluation Field Study (EMEFSII), in central Ontario in March/April 1990. While no single model stands out as being best or worst, the general tendency is that those models simulating the full oxidant chemistry tend to agree best with observations although differences in transport and treatment of clouds are important as well.

## 1. Introduction

Three-dimensional models of atmospheric trace constituents abound since they are important tools in understanding climate, stratospheric ozone depletion, tropospheric oxidants and acidification of ecosystems. Current interest in the role of aerosols in climate makes the processes of chemical transformation in clear air and in clouds precipitation scavenging, dry deposition and stratospheric-tropospheric exchange especially important. Therefore an international effort on comparison of large-scale sulfate models (COSAM) was under-

* Corresponding author.
e-mail: Ulrike. Lohmann@Dal.Ca

taken (Barrie et al., 2001). The rationale for focusing on sulfate was that it was the aerosol component most widely modeled by atmospheric researchers and for which most observations exist. The comparison involved both chemical transport models (CTMs) driven by observed winds and general circulation models (GCMs) that generate their own winds.

The COSAM exercise is described in detail by Barrie et al. (2001). It includes a description of experiment design, participating models and an overview of results. More specifically, the simulation of regional and global budgets is discussed by Roelofs et al. (2001) and Barrie et al. (2001). In this paper a comparison of model simulations with observations of the vertical structure of $SO_2$ and sulfate aerosols near the eastern North American source region is discussed. This is motivated by the outcome from the last intercomparison workshop (Rasch et al., 2000). They concluded: "While most models showed very broad qualitative agreement in species distribution at the surface, the very broad range of results seen in the simulations in the middle and upper troposphere indicates our uncertainty in the mechanisms controlling the tracer distributions there. Their uncertainties can only be reduced by more observations to provide a means of identifying a faulty understanding of particular processes."

Feichter and Lohmann (1999) used a subset of vertical profiles obtained during the North Atlantic Regional Experiment (NARE) to compare a simulation with the ECHAM GCM relaxed to reanalysis data from the European Centre for Medium-Range Weather Forecasts (ECMWF) over the period when the NARE data were taken. They find a reasonable agreement of within $\pm 50\%$ with aircraft observations for simulated variables like wind, temperature and relative humidity which have been nudged to ECMWF data. Variables, however, that show a high temporal and spatial variability, like cloud liquid water and sulfur concentrations are in poorer agreement with observations. A feature nicely captured by ECHAM is that secondary sulfate maxima are often found above maxima in cloud occurrence, indicating that most of the sulfate aloft is formed in clouds.

Barth et al. (2000) compared vertical profiles of $H_2O_2$, DMS, $SO_2$ and $SO_4^{2-}$ from the NCAR GCM to observations obtained during the Pacific Exploratory Mission (PEM) campaign in the Pacific and found reasonable agreement. However, as Barth et al. (2000) note the aircraft data are made over short periods of time and only a few profiles were flown at each location, so that it is not clear to what extent the measurements are representative for that region over a longer period of time. In order to be able to evaluate CTM's and climate models at the same time, measurements are needed that do not depend too heavily on actual wind direction. Thus, the PEM measurements are not ideal for comparing with one grid point monthly average model results. Therefore, we utilize the entire data sets collected during NARE and Second Eulerian Model Evaluation Field Study (EMEFSII) where 46 and 64 profiles were obtained, resp. The number of profiles is comparable to the number of profiles archived over the same time period in the models, which is once or twice daily typically. Observations of vertical profiles of $SO_2$, sulfate aerosols, hydrogen peroxide, ozone and cloud liquid water content were obtained during NARE, which took place in August and September 1993 over the North Atlantic near Nova Scotia (Banic et al., 1996) and during EMEFSII which took place in March and April 1990 near North Bay, Ontario (Issac et al., 1998). $^{222}Rn$ data during NARE are obtained from Zaucker et al. (1996).

A brief description of the models is given in Section 2, and a description of the observational data is given in Section 3. A comparison of modeled and observed vertical profiles during NARE and EMEFSJI as well as simulations of meridional cross-sections are discussed in Section 4. Conclusions are given in Section 5.

## 2. Model description and experimental design

Models may be classified as climatological or episodic, and as on-line or off-line: Chemical transport models (CTM) which calculate the tracer distributions based on a prescribed meteorology are called off-line and general circulation models (GCM) which calculate meteorology and additional chemical species simultaneously are on-line models. CTMs are driven by climatological mean or by instantaneous 6- or 12-hourly wind fields. Wind fields are provided by GCMs or by data assimilation of observed winds as performed at

weather forecast centers (e.g., ECMWF, National Center for Environmental Prediction (NCEP)). GCMs treat the transport of atmospheric constituents similar to that of water vapor by introducing additional prognostic variables on-line with the model's meteorology. Applying a Newtonian relaxation technique, GCMs can be forced to simulate a specific weather episode. This technique, also called nudging, relaxes the model state toward observational data by adding an additional term to the model's equations at each time-step (Jeuken et al., 1996).

In this model comparison exercise, 11 models participated. Four of them are GCMs generating their own transport internally, seven are CTMs, either using analyzed winds or nudging their winds toward reanalysis data from ECMWF. One of the CTMs is a hemispheric CTM while the rest are global models. One GCM (GD) also applies the nudging technique. Climate models were run for 3–5 years and models driven by real winds for at least one year, in most cases from mid 1993 to mid 1994. This period was chosen because they were many high quality routine observations of sulfur compounds at remote stations in the Arctic, North Atlantic, eastern North America and Europe and it covers the NARE period. One model (CD) was included even though it ran for 1997/98 and only simulated $^{222}$Rn and $^{210}$Pb.

A summary of all the models including their dry and wet deposition parameterization, their different model physics and their treatment of oxidants is given in Tables 1–4. The models, simulating sulfur, differ in their horizontal resolution ranging from $5.6^\circ \times 5.6^\circ$ to 150 km by 150 km and between 9 and 31 vertical levels in the vertical. CD has the highest vertical resolution with 46 levels of which about 20 levels are in the troposphere. Half of the models solve prognostic equations for cloud water of large-scale clouds while the other diagnose it. Convection is parameterized with a mass flux scheme in all models except the hemispheric model, which does not parameterize convection at all. While two models use finite differences to calculate advection and two use second order moments, the majority employ semi-Lagrangian advection schemes. Vertical diffusion is either calculated from the mixing-length approach or a prognostic equation for the turbulent kinetic energy is solved.

In addition to simulating the sulfur cycle, $^{222}$Rn and $^{210}$Pb were simulated as outlined in Jacob et al. (1997). The only removal of $^{222}$Rn is its first order radioactive decay rate $2.11 \cdot 10^{-6}\,s^{-1}$ to produce $^{210}$Pb. The removal of $^{210}$Pb is treated as if it were a sulfate aerosol.

The complexity of the treatment of sulfur chemistry in these global models differs considerably. The simplest models only carry prognostic equations for dimethyl sulfide (DMS) and sulfur diox-

Table 1. *Model resolution and references*

| Model code | Full name | Investigator | Resolution | | Meteorology | References |
|---|---|---|---|---|---|---|
| | | | Horizontal | Vertical | | |
| GA | GISS | Koch | $4^\circ \times 5^\circ$ | 9 levels | generated | Koch et al. (1999) |
| GB | ECHAM4-UU | Roelofs | $3.75^\circ \times 3.75^\circ$ | 19 levels | generated | Roelofs et al. (1998) |
| GC | CCCma | Lohmann | $3.75^\circ \times 3.75^\circ$ | 22 levels | generated | Lohmann et al. (1999) |
| GD | ECHAM4-MPI | Feichter, Land, Kjellström | $2.8^\circ \times 2.8^\circ$ | 19 levels | nudged to ECMWF | Feichter and Lohmann (1999) |
| CA | TOMCAT | Bridgeman, Law | $5.6^\circ \times 5.6^\circ$ | 31 levels | ECMWF | Law et al. (1998), Giannakopoulos et al. (1999) |
| CB | KNMI/IMAU | Jeuken, Dentener | $3.75^\circ \times 5^\circ$ | 19 levels | ECMWF | Dentener et al. (1999) |
| CC | MIRAGE | Easter | $2.8^\circ \times 2.8^\circ$ | 24 levels | nudged to ECMWF | Saylor et al. (1999) |
| CD | IMPACT | Bergmann | $2^\circ \times 2.5^\circ$ | 46 levels | GEOS | Penner et al. (1998) |
| CE | GOCART | Chin | $2^\circ \times 2.5^\circ$ | 20 levels | GEOS | Chin et al. (2000) |
| CF | NCAR | Rasch | $1.8^\circ \times 1.8^\circ$ | 26 levels | NCEP | Rasch et al. (1997) |
| HA | DEHM | Christensen | 150 km | 12 levels | ECMWF | Christensen (1997) |

Table 2. *Model physics*

| Model | Full name | Advection | Vertical diffusion | Large-scale clouds |
|---|---|---|---|---|
| GA | GISS | 2nd order moments | none | prognostic |
| GB | ECHAM4-UU | semi-Lagrangian | TKE[1] | prognostic |
| GC | CCCma | semi-Lagrangian | ML[2] | prognostic |
| GD | ECHAM4-MPI | semi-Lagrangian | TKE | prognostic |
| CA | TOMCAT | 2nd order moments | ML | diagnostic |
| CB | KNMI/IMAU | finite differences | ML | diagnostic |
| CC | MIRAGE | finite differences | TKE | prognostic |
| CD | IMPACT | semi-Lagrangian | implicit scheme | diagnostic |
| CE | GOCART | semi-Lagrangian | TKE from GEOS | diagnostic |
| CF | NCAR | semi-Langragian | ML | diagnostic |
| HA | DEHM | pseudospectral advection (hor), finite elements (ver) | ML | prognostic |

[1]TKE: prognostic variable for turbulent kinetic energy.
[2]ML: mixing length approach.

Table 3. *Oxidant chemistry*

| Model | Full name | Gas phase $SO_2$ | Aqueous phase $SO_2$ | $H_2O_2$ | OH | $O_3$ | $NO_3$ |
|---|---|---|---|---|---|---|---|
| GA | GISS | OH | $H_2O_2$ | prognostic | imported | none | imported |
| GB | ECHAM4-UU | OH | $H_2O_2$, $O_3$ | full | full | full | full |
| GC | CCCma | OH | $H_2O_2$, $O_3$ | imported | imported | imported | imported |
| GD | ECHAM4-MPI | OH | $H_2O_2$, $O_3$ | imported | imported | imported | imported |
| CA | TOMCAT | OH | $H_2O_2$, $O_3$ | imported | imported | imported | imported |
| CB | KNMI/IMAU | OH | $H_2O_2$, $O_3$ | full | full | full | full |
| CC | MIRAGE | OH | $H_2O_2$, $O_3$ | [1] | [1] | imported | none |
| CD | IMPACT | [2] | [2] | [2] | [2] | [2] | [2] |
| CE | GOCART | OH | $H_2O_2$ | imported | imported | none | imported |
| CF | NCAR | OH | $H_2O_2$, $O_3$ | prognostic | imported | imported | imported |
| HA | DEHM | param. | param. | none | none | none | none |

[1]CC simulates daytime oxidant chemistry with prescribed ozone and $NO_x$.
[2]CD only simulates $^{222}Rn$ and $^{210}Pb$.

Table 4. *Deposition parameterization*

| Model | $SO_2$ dry deposition | In-cloud scavenging |
|---|---|---|
| GA | RIS[1] (Wesely and Hicks, 1977) | coupled to model's precipitation formation |
| GB | RIS (Ganzeveld et al., 1998) | coupled to model's precipitation formation |
| GC | RIS (Ganzeveld et al., 1998) | Giorgi and Chameides (1986) |
| GD | RIS (Ganzeveld et al., 1998) | Giorgi and Chameides (1986) |
| CA | CV[2] (Muller and Brasseur, 1995) | coupled to model's precipitation formation |
| CB | RIS (Ganzeveld et al., 1998) | coupled to model's precipitation formation |
| CC | CV: $v_d = 0.5$ cm s$^{-1}$ everywhere | coupled to model's precipitation formation |
| CD | RIS (Wesely and Hicks, 1977) | Giorgi and Chameides (1986) |
| CE | RIS (Wesely and Hicks, 1977) | Giorgi and Chameides (1986) |
| CF | RIS (Wesely and Hicks, 1977) | coupled to the model precipitation formation |
| HA | RIS (Voldner et al., 1986) | coupled to the model precipitation formation |

[1]RIS: resistance in series.
[2]CV: constant velocity.

ide ($SO_2$) gases and sulfate ($SO_4^{2-}$) aerosol, and import three-dimensional monthly mean oxidant concentrations simulated by models with detailed oxidant chemistry (e.g., Feichter et al. (1996) or Lohmann et al. (1999)). Some consider an additional pathway of DMS oxidation to form methane sulfonic acid (MSA) (Chin et al. (1996) or Pham et al. (1995)).

Currently there exist three approaches for the treatment of hydrogen peroxide ($H_2O_2$) which is the most important oxidant of $SO_2$. The simplest one is using prescribed $H_2O_2$ concentrations (e.g., Feichter et al. (1996)). Recently some groups (e.g., Barth et al. (2000), Koch et al. (1999)) started to solve a simplified prognostic approach for $H_2O_2$ with prescribed $HO_2$ concentrations, where the source of $H_2O_2$ is prescribed and the sink of $H_2O_2$ is calculated due to scavenging and aqueous phase oxidation with $SO_2$ to form sulfate. In this approach hydroxyl radical (OH) and the photolysis rate of $H_2O_2$ need to be prescribed to calculate $H_2O_2$ destruction as well as the peroxide radical ($HO_2$) to calculate $H_2O_2$ production. The most sophisticated models simulate $H_2O_2$, ozone ($O_3$), OH and nitrogen dioxide ($NO_2$) prognostically and include simplified schemes for some of their precursors (Roelofs et al. (1998), Dentener et al. (1999)).

Half of the CTMs calculate a rather complex oxidant chemistry as described above (referred to as full oxidant chemistry in Table 3), whereas most GCMs prescribe monthly mean values for $H_2O_2$, $O_3$, OH and $NO_2$. Nitrate ($NO_3$) is then calculated from $NO_2$ and $O_3$ applying equilibrium conditions.

Dry deposition is parameterized using the analogy to resistance in series (Ganzeveld et al. (1998), or Wesely and Hicks (1977)) in all but two models which use a constant dry deposition velocities. The resistance in series approach distinguishes different surface types in the calculation of aerodynamic resistance. It depends also on windspeed and atmospheric stability. Typical values of dry deposition velocities for $SO_2$ are 0.2–0.4 cm $s^{-1}$ over land and 0.8 cm $s^{-1}$ over the oceans using the parameterizations cited above whereas, for instance, model CC uses a constant velocity for $SO_2$ of 0.5 cm $s^{-1}$ everywhere.

Most of the models treat the in-cloud scavenging consistent with the model's cloud physics, that is, using the ratio of precipitation formation to cloud water concentration as the scavenging rate. Treatment of below-cloud scavenging varies greatly among the models. Some models use a rather simple approach, that is they apply Giorgi and Chameides (1986) for in-cloud scavenging based on a cloud liquid water content of 0.5 μg $m^{-3}$ and follow Berge (1993) for below-cloud scavenging. The majority of models distinguishes between convective and large-scale scavenging.

## 3. Data description

### 3.1. North Atlantic Regional Experiment (NARE)

One set of observational data is taken from the 1993 NARE intensive. The data were collected from the National Research Council of Canada (NRCC) DHC-6 Twin Otter aircraft from 9 August to 8 September 1993. Profiles were made between points about 50 km south of Yarmouth, Nova Scotia (about 43.3°N, 66°W) and inland over Kejimikujik National Park, Nova Scotia (about 44.3°N, 65.5°W). The flights were conducted at least 6 days a week and back-trajectories analysis indicates that the air arrived from a variety of origins (Merrill and Moody, 1996).

Details of the instrumentation and observations, as well as other analyses of the NARE data, are described in a number of papers in a special section of the *Journal of Geophysical Research* (Fehsenfeld et al., 1996; Banic et al., 1996). A few aspects of the instrumentation are repeated here in brief.

All trace gas measurements were recorded at 1 s intervals. $SO_2$ was measured with a TECO 43S pulsed fluorescence monitor. The detection limit for $SO_2$ for a 1 s measurement is 0.2 ppbv and the uncertainty is $\pm$(0.1 ppbv + 30% of measurement). $O_3$ was measured with a TECO 49 UV absorption analyzer. The uncertainty is $\pm$(5 ppbv $\pm$10% of measurement). $H_2O_2$ was measured using the Kok method and Fenton reagent chemistry. The detection limit is about 0.1 ppbv and the uncertainty is about 5%. For more details concerning these measurements, the reader is referred to Banic et al. (1996) and Weinstien-Lloyd et al. (1996).

Mass concentrations of sulfate were measured using ion chromatography of integrated aerosol samples collected on Teflon filters. Continuous

measurements of the mass concentration of sulfate are not available directly from the measurements. However Banic et al. (1996) showed that the mass concentrations of $SO_4^{2-}$, measured from the exposed filter samples, were highly correlated with the number concentrations of particles in the 7th channel of the Particle Measuring Systems (PMS) Passive Cavity Aerosol Spectrometer Probe (PCASP) $-100X$ that was mounted under a wing of the aircraft. Channel 7 of this PCASP corresponds to particles of about $0.38\ \mu m \pm 0.05\ \mu m$ diameter. A fourth order polynomial fit constrained through the origin was fit to the data. This level of detail in the fit, shown in Fig. 1, was used to ensure an adequate representation of the data at lower concentrations. The polynomial fit of Fig. 1 was used to derive 1 s values of $SO_4^{2-}$ mass concentration. The standard error of the PCASP-$SO_4^{2-}$ relationship is $0.48\ \mu g\ m^{-3}$ for $SO_4^{2-} < 3\ \mu g\ m^{-3}$ and $2.3\ \mu g\ m^{-3}$ for $SO_4^{2-}$ between 6 and $31\ \mu g\ m^{-3}$, the range appropriate to the observations. This is much less than the standard error of the observations.

The effect of cloud was removed from the dataset by excluding data when the corresponding number concentration of particles measured with the PMS FSSP-100 (2–35 μm) was greater than $5\ cm^{-3}$. It is assumed that such concentrations do not occur outside of cloud.

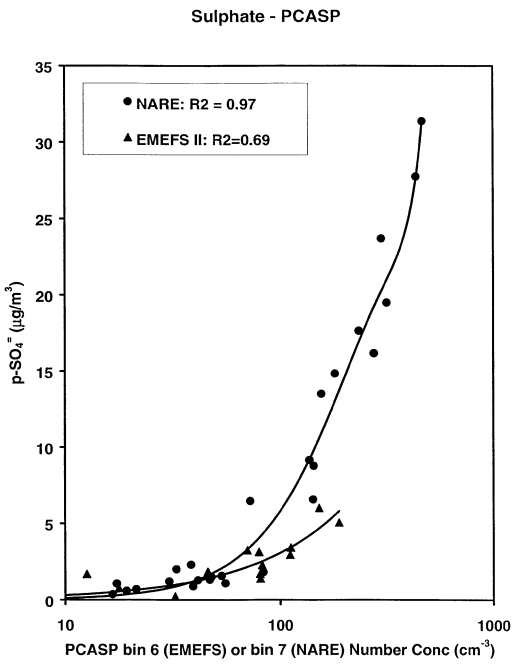


*Fig. 1.* Regression between PCASP and sulfate for NARE and EMEFSII.

The data for $O_3$, $H_2O_2$, $SO_2$ and $SO_4^{2-}$ for 31 profiles to approximately 3 km made on 23 days and 15 profiles to 5 km made on 14 days are shown in Fig. 2. For each 5 km profile there are approximately 1500 data points. The average profile in each plot was derived by ordering all the 1 s data from the profiles by altitude and then taking the average of all points within selected altitude intervals. The intervals were taken from the pressure intervals used in the Canadian Regional Climate Model. The impact of setting the below detection limit (BDL) values for $SO_2$ to zero before computing averages, as opposed to using the indicated values, is small; the total column $SO_2$ for the 5-km profiles computed by leaving the BDL values as measured is less than 1% higher than that derived from setting the BDL values to zero. Both the 3-km and 5-km profiles are used in the model intercomparison. It is assumed that the combination of the two groups of profiles, which cover most of the measurement days, represents the average characteristics of the entire period, as has been discussed by Banic et al. (1996).

### 3.2. *Second Eulerian model evaluation field study (EMEFSII)*

A second set of observational data is taken from the Canadian component of EMEFSII. The study was conducted from 20 March to 29 April 1990 again using the NRCC DHC-6 Twin Otter aircraft. The aircraft was based out of North Bay, Ontario and profiles were made over two ground-based observation sites at Egbert, Ontario (44.2°N, 79.8°W) and Lake Traverse, Ontario (45.9°N, 78.1°W). Details of the study and instrumentation are given by Issac et al. (1998). Again, a few aspects of the instrumentation are briefly outlined below.

All trace gas measurements were recorded at 1 s intervals. $SO_2$ was measured with a TECO 43S pulsed fluorescence monitor. The detection limit for $SO_2$ for a 1 s measurement was 0.3 ppbv and the uncertainty is $\pm$(0.1 ppbv + 30% of measurement).

Again, because continuous measurements of the

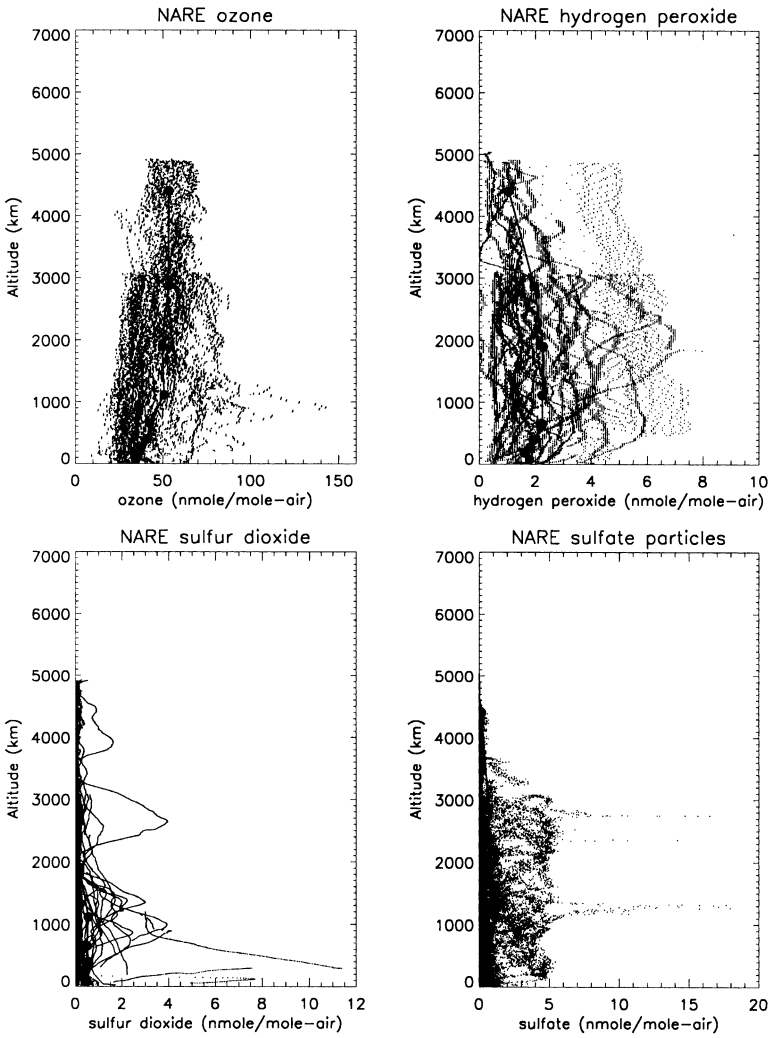


*Fig. 2.* Individual and average vertical profiles of $O_3$, $H_2O_2$, $SO_2$ and $SO_4^{2-}$ obtained during NARE from 31 profiles to approximately 3 km on 23 days and 15 profiles to 5 km over 14 days.

mass concentration of sulfate were not available directly from the measurements, high-resolution sulfate concentrations were derived using the PCASP number concentrations as a surrogate. A good correlation between the mass concentrations of sulfate, measured using ion chromatography on aerosol samples collected on Teflon filters, and channel 6 of the PCASP was found for flights during the period 8 April–15 April 1990. The constrained time period is due to problems with the PCASP operation. The data and fitted curve are also shown in Fig. 1.

The effect of cloud was removed from the dataset by excluding data when the corresponding number concentration of particles measured with the FSSP-100 (2–35 μm) was greater than 5 $cm^{-3}$.

The $SO_2$ data are taken from 34 profiles over Egbert and 30 profiles over Lake Traverse on 24 days. Because of the PCASP limitations, the $SO_4^{2-}$ data are from 14 profiles over Egbert and

10 profiles over Lake Traverse on 7 days. Compilations of the profiles for each constituent are shown in Fig. 3 for Egbert and Lake Traverse. The data were processed as for NARE but separated by location. This was done because Egbert and Lake Traverse are about 230 km apart. For air traffic reasons, about 80% of the profiles over Egbert were restricted to about 3 km, whereas 90% of the profiles made over Lake Traverse profiles extended up to 5 km or higher. The average profiles for both the Egbert and Lake Traverse measurements are used in the intercomparison.

### 3.3. Column burdens

The column burdens of $SO_2$ and $SO_4^{2-}$ for the average measured profiles are given in Table 5 for both datasets. For NARE, most of the total sulfur burden is in the lower 3 km. Most of the sulfur above 3 km is in the form of $SO_2$. Overall, about 75% of the NARE sulfur is as sulfate. For

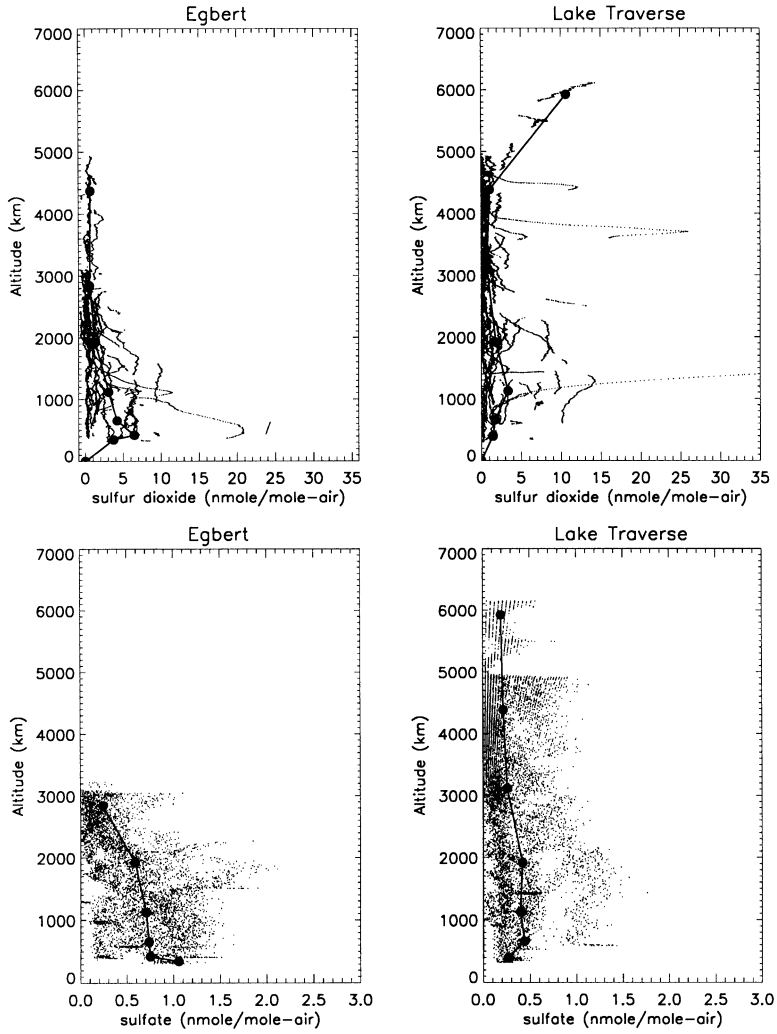


*Fig. 3.* Individual and average vertical profiles of $SO_2$ and $SO_4^{2-}$ obtained during EMEFSII. Profiles of $SO_2$ are from 34 profiles over Egbert and 30 profiles over Lake Traverse on 24 days each. Profiles of $SO_4^{2-}$ are from 14 profiles over Egbert and 10 profiles over Lake Traverse on 7 days each.

Table 5. *Observed average column Burdens at NARE and EMEFSII ($\mu g\, m^{-2}$ of S)*

| Location | $SO_2$ burden | $SO_4^{2-}$ burden | $SO_2 + SO_4^{2-}$ burden |
|---|---|---|---|
| NARE | | | |
| 0–3 km profiles, 0–3 km burden | 1110 | 3020 | 4130 |
| 0–5 km profiles, 0–5 km burden | 1310 | 3040 | 4340 |
| 0–5 km profiles, 0–3.8 km burden | 1250 | 3005 | 4255 |
| EMEFSII | | | |
| Egbert, 0–6 km burden | 8000 | 1870 | 9870 |
| Egbert, 0–3.8 km burden | 7230 | 1870 | 9100 |
| Lake Traverse, 0–6 km burden | 12180 | 1740 | 13920 |
| Lake Traverse, 0–3.8 km burden | 6790 | 1360 | 8150 |

EMEFSII, the ReDoubt volcano in Alaska contributed largely to the middle troposphere of $SO_2$. With that contribution removed (i.e., below 3.8 km), the difference between Egbert and Lake Traverse is reduced. In contrast to the summertime NARE, $SO_2$ was much higher than sulfate in the winter–spring EMEFSII, accounting for 80% or more of the total sulfur. Also, the EMEFSII total sulfur burden is more than twice that of NARE. We remind that the $SO_4^{2-}$ data are only from 7 days, whereas $SO_2$ is from 23 days.

## 4. Results

### 4.1. *Meridional transects of modeled sulfur in eastern North America*

Meridional cross-sections along different longitudes were archived from the models in order to compare the differences between them. Figs. 4–7 show cross-sections along 80°W during Northern Hemispheric winter (DJF) and summer (JJA) of $SO_2$ and $SO_4^{2-}$ mixing ratio. Differences between models are evident.

For $SO_2$ in DJF, there is a marked peak in mixing ratio in the lower troposphere of mid to high latitudes. The highest resolution model HA is used here as a reference since it agrees very well with surface observations throughout the northern hemisphere (Christensen, 1997; Barrie, et al., 2001). There are two peaks in $SO_2$: one at 30–60°N associated with the eastern North American source region and one in the Arctic associated with long range transport of $SO_2$ to the Arctic from Eurasia (Barrie, 1996; Christensen, 1997). Although most models capture the source region peak at mid-latitudes not all show a distinct maximum in the high Arctic. Some (GC, GD) agree with HA. Others show elevated $SO_2$ levels but fail to separate the Arctic peak from the eastern North American peak (GA, GB, CB, CE, CF). Two models show almost no Arctic peak at all (CA, CC). The above differences are largely explained by differences in $SO_2$ oxidation rather than in transport. Barrie et al. (2001) show that CA and CC oxidize $SO_2$ too much in high northern winter latitudes while GA, GB, CE and CF do not oxidize enough. GC, GD and HA (the reference) are similar. These differences in $SO_2$ oxidation deduced from the Arctic peak also help explain differences in the mid-latitude eastern North American peak.

All global models simulate one to two maxima above 3 km in the tropics, the magnitude of which varies considerably between the models depending on the location and parameterization of convective events and wet deposition. $SO_2$ concentrations exceed 1 ppbv in convective plumes in CE and CF while the core values are below 0.5 ppbv in GB.

Large discrepancies of $SO_2$ at the surface are expected to result from differences in the parameterization of dry deposition velocity (cf. Table 4). Only CA and CC prescribe a constant dry deposition velocity everywhere while all the other models use a surface dependent resistance depending on atmospheric stability and surface type. Therefore they deposit more $SO_2$ over snow at high latitudes than the surface dependent schemes resulting in a lower $SO_2$ concentration near the surface (Fig. 4).

In northern/boreal winter, most sulfur is in the form of $SO_2$, so that $SO_4^{2-}$ concentrations on the Northern Hemisphere are much smaller than $SO_2$ concentrations. The $SO_4^{2-}$ meridional transect in

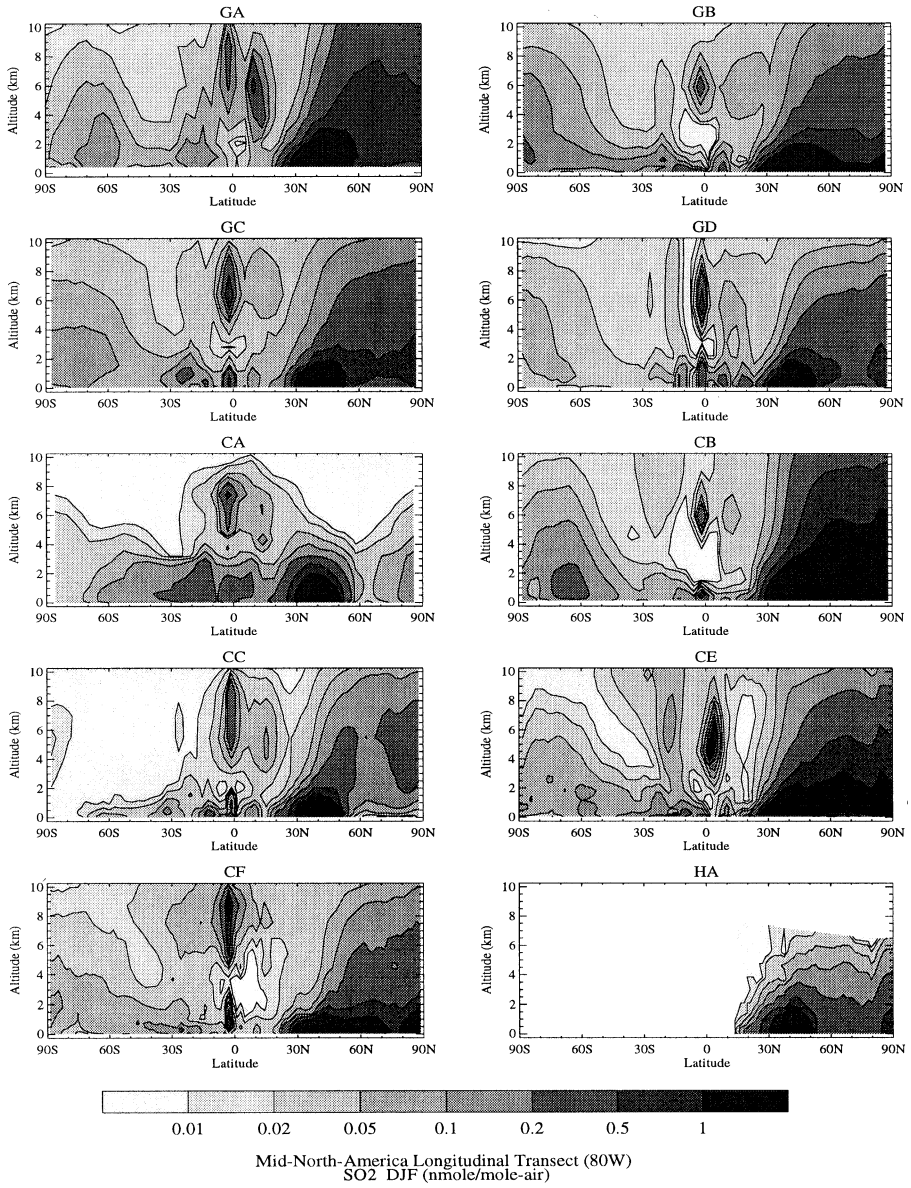


*Fig. 4.* Meridional cross-section of $SO_2$ along 80°W for DJF.

DJF through eastern North America pole to pole (Fig. 5) is consistent with differences in the models deduced from the $SO_2$ transect. Models CC and CA overpredict $SO_4^{2-}$ in the Arctic while GA, GB, CB, CE and CF underpredict. GD and HA are similar. Here GC has shifted to the overprediction of $SO_4^{2-}$, which is mainly a result of more transport to the Arctic. Maxima in the free troposphere in the tropics associated with deep convective activity are less pronounced than for $SO_2$ and hardly visible in the simulations with GB and CC.

In northern hemispheric summer, the 80°W meridional transect for $SO_2$ (Fig. 6) is quite different than in winter (Fig. 4). At mid latitudes, a

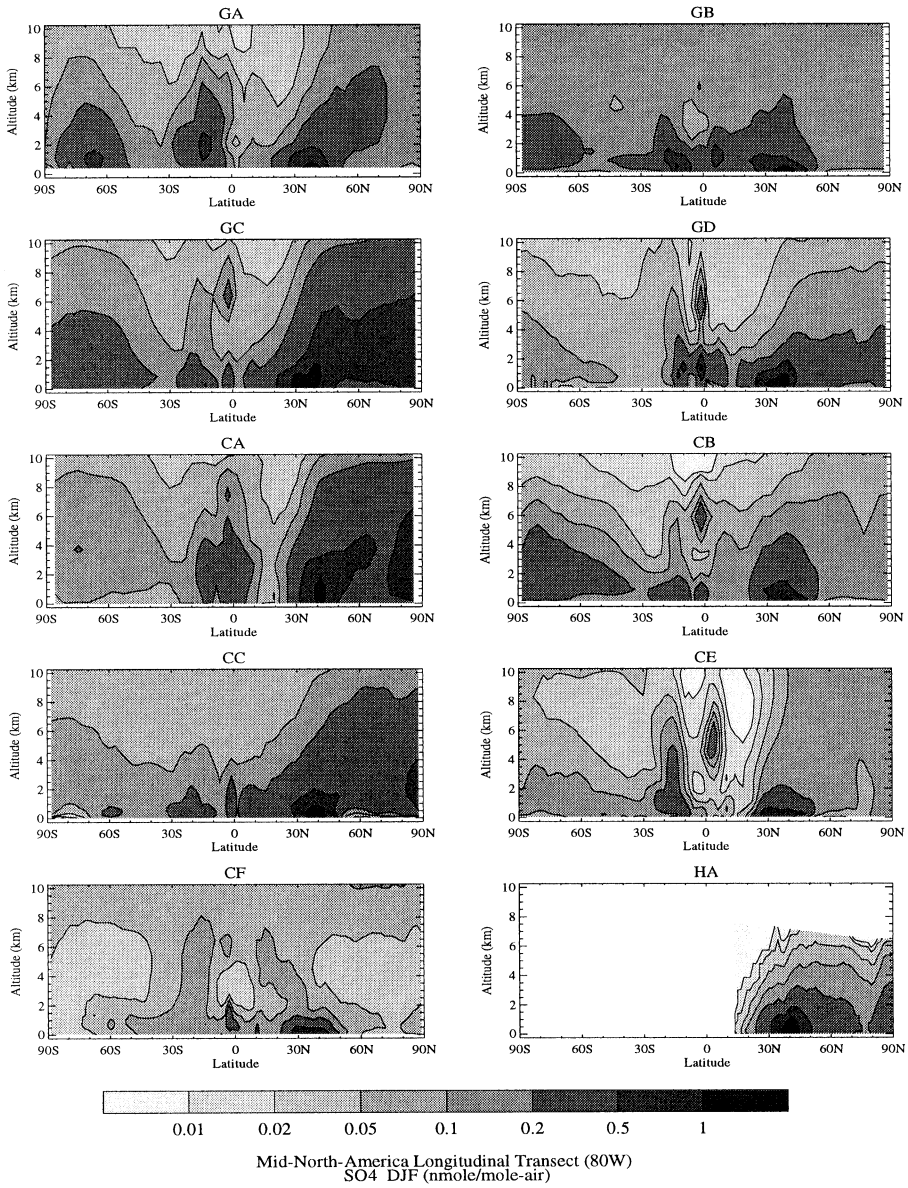


*Fig. 5.* Meridional cross-section of $SO_4^{2-}$ along 80°W for DJF.

peak in $SO_2$ mixing ratio over eastern North America is evident while no peak appears in the Arctic. The latter is consistent with a higher rate of $SO_2$ oxidation and $SO_x$ removal in summer as well as lower transport between Eurasian sources and the Arctic (Barrie, 1996; Christensen, 1997). In contrast to winter, the mid-latitude peak in $SO_2$ is not confined to the lower troposphere in most models. Vertical transport by summertime convection and vertical advection causes rather high concentrations of $SO_2$ all the way up to the tropopause in all models in the tropics. The strongest maxima with core values above 0.5 ppbv above 6 km are simulated in CE and CF. In the upper

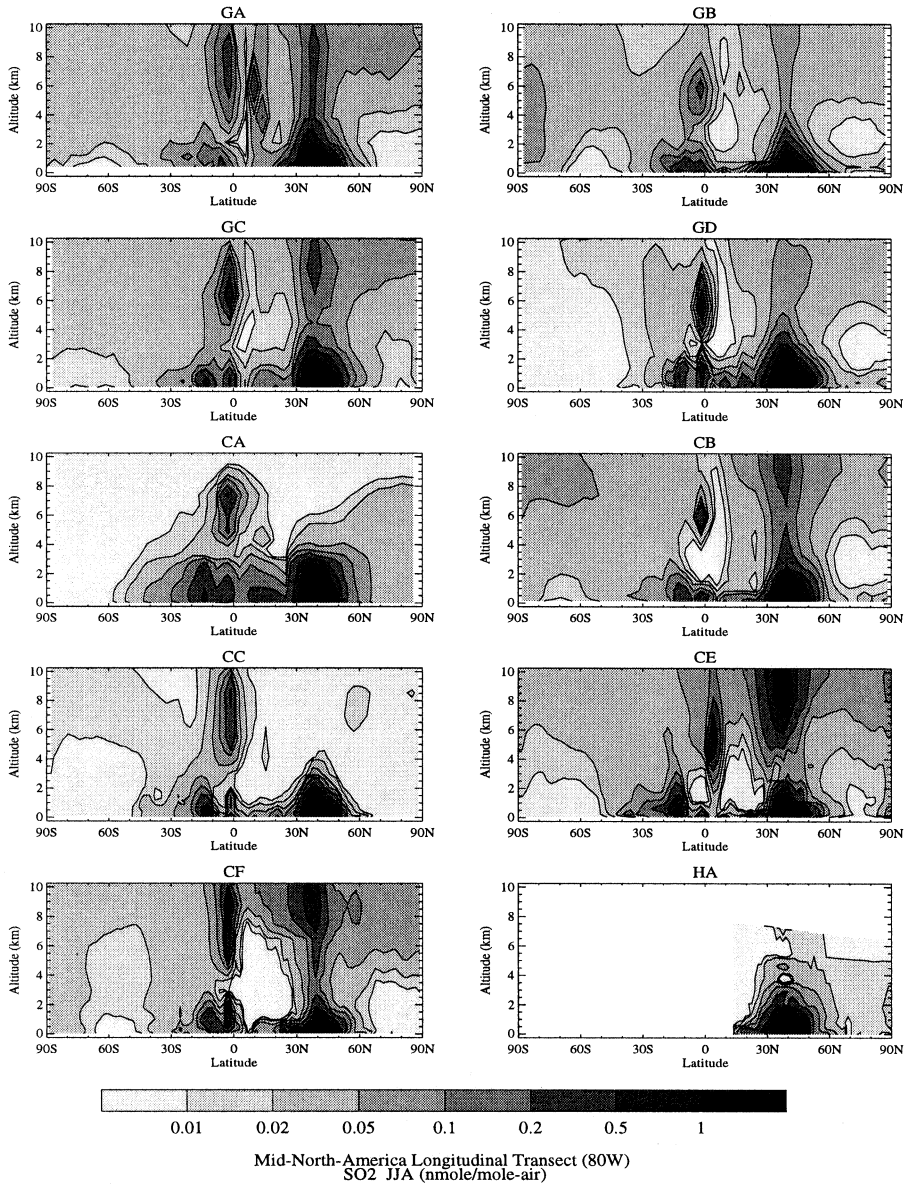


*Fig. 6.* Meridional cross-section of $SO_2$ along 80°W for JJA.

troposphere these models show higher mixing ratios in high latitudes as well. CA, CC and to a lesser extent GD do not show an upper tropospheric mid-latitude secondary peak. Convective activity is also responsible for upper tropospheric maxima between the equator and 30°S which are visible in all models. $SO_2$ concentrations south of 40°S are generally below 0.05 ppbv in all models. As GB and GD employ the same convection scheme, their differences in the strength of the upper tropospheric maxima are related to the mode of operation, employing nudging in GD and using GCM winds in GB. Nudging acts to change the frequency and

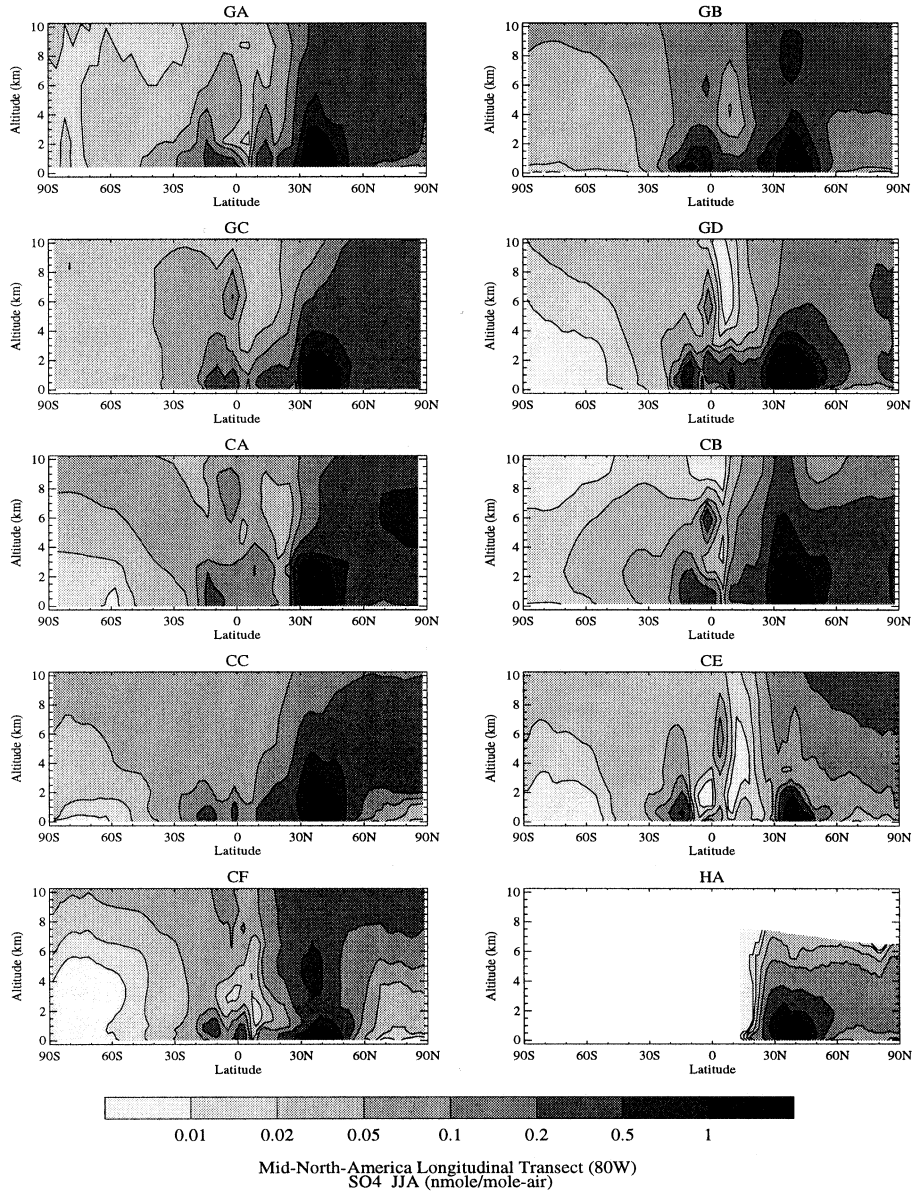


*Fig. 7.* Meridional cross-section of $SO_4^{2-}$ along 80°W for JJA.

location of convection in ECHAM as shown in Jeuken et al. (1996).

For $SO_4^{2-}$ in northern hemispheric summer (Fig. 7) the meridional profile pole-to-pole through eastern North America shows much variation between models. All models capture the mid-latitude source region peak over eastern North America quite consistently. Differences in the upper troposphere mid-to-high latitudes are consistent with a model's ability to vertically transport $SO_2$ and to oxidize it. Thus, GA, GB, GC, CB, CE and CF, but not GD, CA and CC show upper level $SO_4^{2-}$ consistent with vertical transport of $SO_2$. CA is most pronounced in showing a general

feature, namely, a poleward tilt in the relatively long-lived oxidation product of $SO_2$. This leads to a secondary maximum of $SO_4^{2-}$ in the summer upper tropospheric Arctic. A common feature in GB, CA, CC and CF is that $SO_4^{2-}$ concentrations exceeding 0.05 ppbv are found in the upper Antarctic troposphere. Wet deposition in convective clouds seems to be very dominant in CE, which is the only model with a distinct minimum between 30°N and 10°S.

### 4.2. The NARE case study

Simulated vertical profiles of $SO_2$, sulfate aerosols, hydrogen peroxide and liquid water content are compared with observations at the sites of the field experiments NARE and EMEFSII. The model results are averages over the period of the case studies of samples taken every 6 to 12 h depending on the output interval of the models. Prior to the comparison of $SO_2$ and $SO_4^{2-}$ we show vertical profiles of $^{222}Rn$ and $^{210}Pb$ at the NARE site, as an indication of how different the transport and scavenging in case of $^{210}Pb$ is between the models.

Surface $^{222}Rn$ concentrations (Fig. 8) vary from 20 to over $80 \times 10^{-21}$ mole mole-air$^{-1}$ between the models while an average over the observations yields $25 \times 10^{-21}$ mole mole-air$^{-1}$ increasing to $40 \times 10^{-21}$ mole mole-air$^{-1}$ at 1 km. The global, annual burden of $^{222}Rn$ agrees to within 20% between the models, but regional discrepancies are much larger due to differences in emission over land and ocean, i.e., due to the characterization of land and sea around Nova Scotia. Differences above the surface are caused by differences in vertical and horizontal transport (convective and advective), as the radioactive decay rate of $2.11 \cdot 10^{-6}\,s^{-1}$ is the only sink in all models. Large differences also occur in the standard deviation of $^{222}Rn$. None of the models simulates the observed $^{222}Rn$ inversion above the surface, but

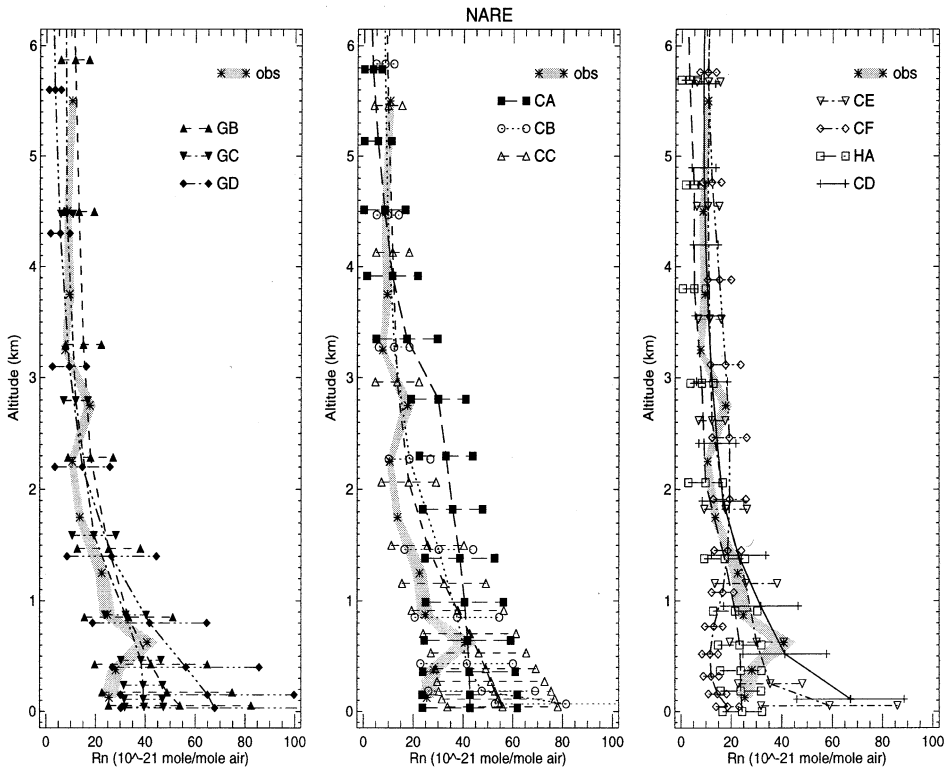


*Fig. 8.* Vertical profile of $^{222}Rn$ ($10^{-21}$ mole mole-air$^{-1}$) $\pm$ one standard deviation obtained during NARE from the different models and observations (Zaucker et al., 1996).

on the contrary in most models $^{222}$Rn concentration rapidly decreases with height. Only in GC, CA and HA $^{222}$Rn is well-mixed within the boundary layer. These differences near the ground are mainly due to the different PBL mixing schemes (cf. Table 2). The modelled $^{222}$Rn concentrations $\pm$ one standard deviation overlap with the observed $^{222}$Rn concentrations for all models but CA above 1 km and CF below 1 km. In summary, it is not simply that the models driven with observed winds for the NARE period (GD, CA, CB, CC, CE, CF, HA) are superior to the GCMs generating their own winds but differences in transport parameterization seem to be more important.

The profiles of $^{210}$Pb differ more between the models (Fig. 9) than those of $^{222}$Rn as the removal processes of $^{210}$Pb, especially wet deposition, are treated differently in the participating models. Moreover, $^{222}$Rn does not have a surface deposition loss, its life time is half of that of $^{210}$Pb and its source is primary (surface emission) while that of $^{210}$Pb is secondary (production from $^{222}$Rn decay). Most models show a maximum of $^{210}$Pb above the boundary layer. In GB, GD, CB, CC and CE, where $^{222}$Rn strongly decreases with height, $^{210}$Pb is removed very efficiently near the surface and peaks at the top of the boundary layer. While $^{210}$Pb decreases with height above the boundary layers in most models, it actually increases slightly in CD up to an altitude of 6 km. The $^{210}$Pb concentration in CD does begin to decrease sharply at an altitude of 8–10 km. This is likely caused by efficient scavenging of $^{210}$Pb at low altitudes and strong convection, which pumps $^{222}$Rn and $^{210}$Pb high up. Furthermore, differences in vertical exchange play a role. Models with a rather vigorous vertical exchange like CF, GC and HA have a peak in $^{210}$Pb at higher altitudes than those with a rather weak vertical exchange.

As the most important pathway for sulfate aerosol formation is by aqueous phase oxidation

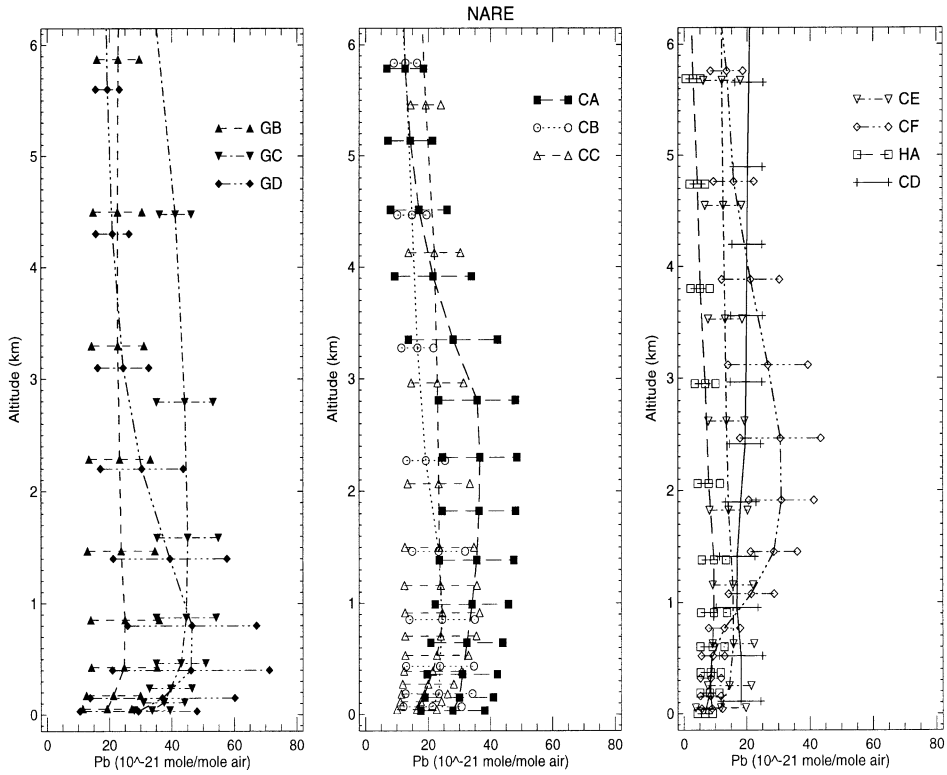


*Fig. 9.* Vertical profile of $^{210}$Pb ($10^{-21}$ mole mole-air$^{-1}$) $\pm$ one standard deviation obtained during NARE from the different models.

of $SO_2$ with $H_2O_2$ and $O_3$, we will show oxidant concentrations ($H_2O_2$ and $O_3$) as well as liquid water content from observations and the models for which this information is available. Also, OH concentrations are compared between the models.

In general, $H_2O_2$ will be produced in favor of ozone when nitrogen oxide concentrations are low. Its distribution is also governed by the distribution of clouds as it is highly soluble. Therefore, one can expect models which calculate ozone and $H_2O_2$ using full oxidation schemes which depend on nitrogen oxide and cloud cover to do best in simulations of these trace gases.

Observed $H_2O_2$ concentrations, as shown in Fig. 10, range from 1.8 ppbv at the surface to 2.3 ppbv at 2 km and decrease aloft to 1 ppbv at 4.4 km. A convexly shaped concentration profile is evident in three models using monthly mean data of $H_2O_2$ (GC, GD, CE), but not in CA. GA and GB which prognose some oxidants (cf. Table 3) also simulate a convex shape. CB and CC, which solve prognostic equations for $H_2O_2$, show very little variation of $H_2O_2$ with height above the boundary layer. Their means plus one standard deviation are lower than the observed mean values below 3 km but fall within the observed variability. GC and GD, which both use monthly mean distributions of $H_2O_2$, underestimate $H_2O_2$ by a factor of two whereas GA and GB, which solve prognostic equations for $H_2O_2$, simulate higher $H_2O_2$ concentrations, in closer agreement with observations. It is interesting to note that all models underestimate $H_2O_2$ and that CF employing a fairly simple prognostic treatment of $H_2O_2$ is closest to observations.

As shown in Fig. 11, observed $O_3$ concentrations range from 35 ppbv at the surface to 50 ppbv at 1 km. Above 1 km, $O_3$ is almost constant with height up to 4.4 km, where the observations stop. All models reproduce the values at the surface well but tend to underpredict ozone by 10 to 20 ppbv above 1 km altitude. However, since

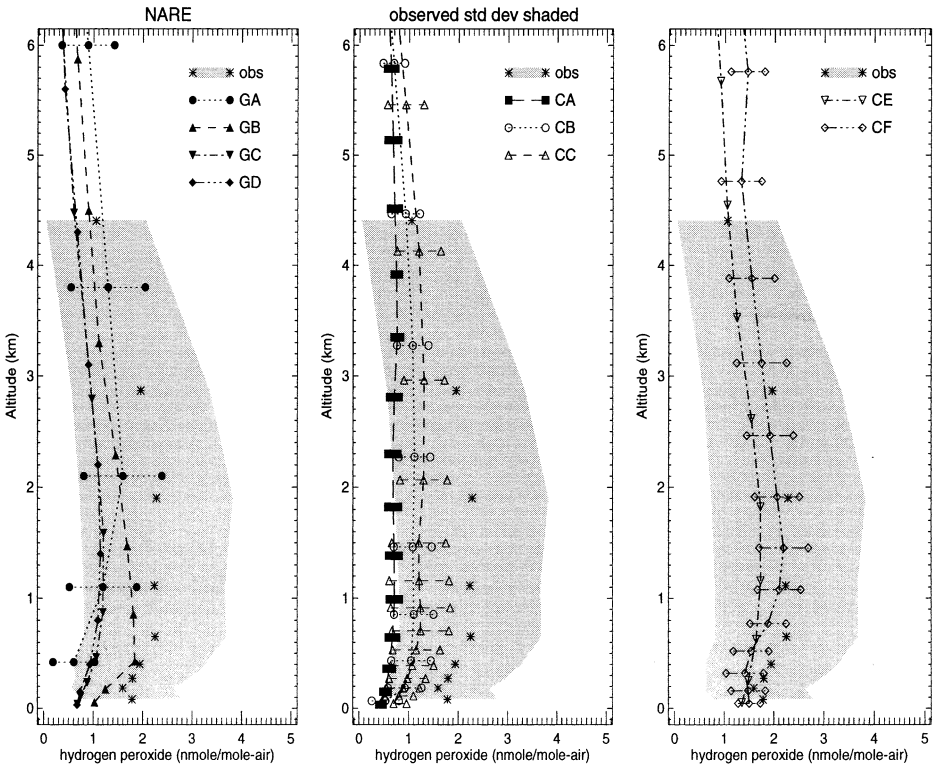


*Fig. 10.* Vertical profile of $H_2O_2$ (ppbv) $\pm$ one standard deviation obtained during NARE from the different models and observations.

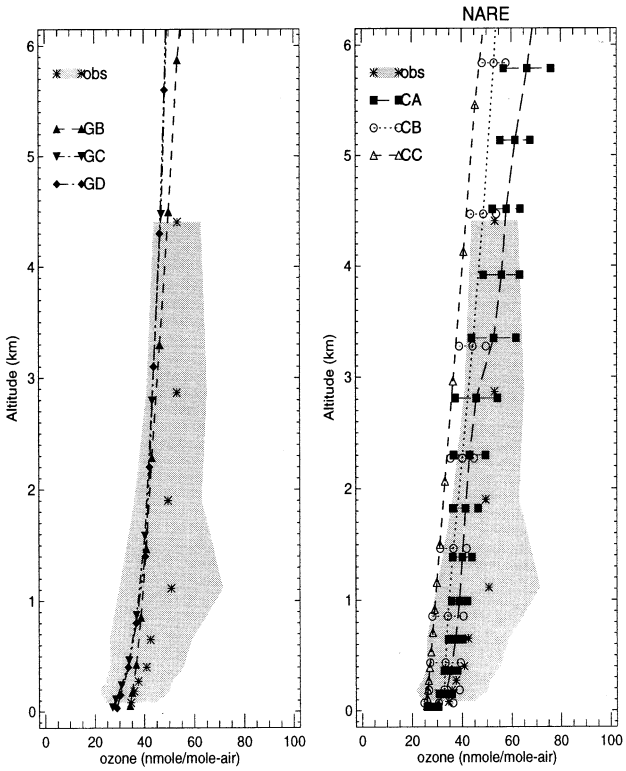


*Fig. 11.* Vertical profile of ozone (ppbv) $\pm$ one standard deviation obtained during NARE from the different models and observations.

oxidation in NARE is in a largely acidic environment $H_2O_2$ rather than ozone likely dominates net $SO_2$ aqueous phase oxidation. Thus, this bias is not too important in the present context.

The clear-sky oxidant OH is shown in Fig. 12 from most models. OH varies considerably between the models ranging from 30 to $170 \times 10^{-15}$ mole mole-air$^{-1}$ near the surface and from 70 to $180 \times 10^{-15}$ mole mole-air$^{-1}$ at 6 km. Only 5 out of 8 models show the anticipated increase of OH with height due to its photochemical source.

Clouds are present most of the time between the surface and 3 km (Fig. 13). The liquid water content (LWC) from the models is an average over the grid box and over clear and cloudy time steps. The maximum observed LWC is 30 mg kg$^{-1}$ at 500 m a result of frequent marine stratus clouds at the NARE location. None of the models except CF shows the strong LWC peak below 1 km. Above 1 km, most of the models (except CA and CC) simulate LWC within the standard deviation of the observations. Due to the coarse vertical model resolution, the height of maximum LWC might be displaced by one vertical level. However, vertical resolution cannot explain everything as CC has a higher resolution in the boundary layer than, for instance, CB but it simulates a much higher liquid water content than observed.

Fig. 14 shows that the observed $SO_2$ mixing ratio during NARE increases from 0.3 ppbv at the surface to 0.6 ppbv at 400 m. It exhibits a secondary peak at 1.1 km and rapidly decreases with height aloft. The peak in $SO_2$ at 400 m is related to the marine boundary layer as the air below 1 km has southerly and easterly trajectories whereas the air above is from the west. The models reproduce this feature more because of dry deposition and less because they mimic the vertical wind shears well. Half of the models overestimate the $SO_2$ mixing ratio up to a factor of three below 2 km, but the simulated mean values from all

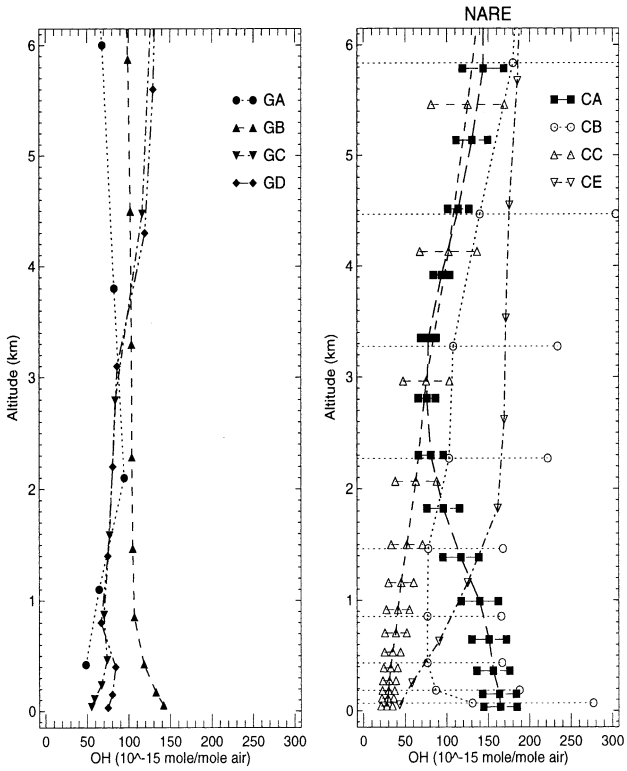


*Fig. 12.* Vertical profile of OH ($10^{-15}$ mole mole-air$^{-1}$) $\pm$ one standard deviation obtained during NARE from the different models.

models except CA are within the standard deviation of the observations. Generally speaking, the higher $H_2O_2$ and the higher the cloud liquid water content, the more $SO_2$ is oxidized to sulfate. Thus, CF which simulates the highest $H_2O_2$ and highest liquid water contents near the surface simulates the lowest $SO_2$ mixing ratios at NARE. On the other hand, CA simulates almost the lowest $H_2O_2$ mixing ratios and its clouds only occupy the layers between 1.5 and 4 km, so that its simulated $SO_2$ mixing ratios at NARE are highest.

Additional differences are caused by the coastal location, where the wind direction is very crucial for the advected trace gas mixing ratio as well as the location of the grid box with respect to land/ocean points. Advection does not seem to be the major reason for the disagreement amongst models, because the results from models driven with observed winds are not superior to those using their own generated winds. The hemispheric model (HA), which is run at a much higher horizontal and temporal resolution and uses a parameterized $SO_2$ oxidation, captures the vertical profile of $SO_2$ very well. Its mean values deviate by less than a factor of two from the observations everywhere. GB, which calculates the full oxidant chemistry also is within a factor of two of the observations everywhere. These models are followed by CB, the chemical transport model which calculates the full oxidant chemistry and GA, the GCM which prognoses $H_2O_2$, which only deviates at one altitude by more than a factor of two from the observations.

As shown in Fig. 15, $SO_4^{2-}$ mixing ratios during NARE are 1 ppbv below 3 km as an average over all flights with a maximum of 1.1 ppbv at 1.1 km. The hemispheric model agrees best with the observations, whereas half of the other models underestimate or overestimate the $SO_4^{2-}$ mixing ratios at some altitudes by more than a factor of two. Only CF predicts $SO_4^{2-}$ mixing ratios less than half of the observed. As CF also simulates low

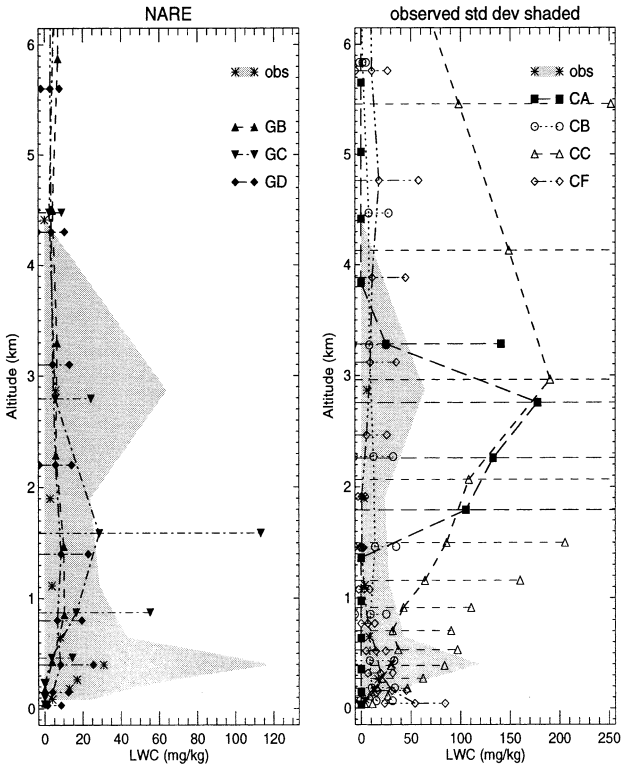


*Fig. 13.* Vertical profile of liquid water content (mg kg$^{-1}$) $\pm$ one standard deviation obtained during NARE from the different models and observations.

$^{210}$Pb concentrations in the lowest 1 km, the most likely cause is the efficient wet deposition of both species caused by precipitation formation from the high liquid water content near the surface. On the other hand, GC and GD simulate more than twice the observed $SO_4^{2-}$ mixing ratios at some altitudes. This is due to insufficient wet scavenging because they have the highest $^{210}$Pb concentrations. In summary, due to the high variability the observed and simulated standard deviations overlap at all altitudes for all models.

The models GC, GD and CA overestimate both $SO_2$ and $SO_4^{2-}$ and, at the same time, show the largest $^{210}$Pb mixing ratios above 500 m. This suggests too little wet deposition. Even though the liquid water content in GC and GE seems to have the right order of magnitude compared with observations, the maximum LWC is displaced in altitude. In GC, the maximum LWC is at 1.6 km, so that aerosols and precursor gases are carried aloft further than observed before subject to in-cloud scavenging. The contrary is seen in CF where LWC peaks at the surface. Moreover, the frequency of occurrence might be different between the observed and simulated clouds. Also, a correctly simulated LWC does not mean that precipitation and wet deposition are correctly reproduced as well. An overestimate of both $SO_2$ and sulfate might also be due to an overestimate of horizontal transport from nearby source regions.

A summary of model performance in terms of column burden of sulfur species is given in Table 6. To obtain column burdens from the different models an air density of 1 kg m$^{-3}$ was assumed. Six (seven) out of the ten models are within a factor of two of the observed column $SO_2$ ($SO_4^{2-}$) burden below 3.8 km. $SO_2$ contributes 25–30% to the total sulfur column burden in the observations. The $SO_2$ contribution is captured within a factor of two in most models, except for CE which underestimates $SO_4^{2-}$ by more than a

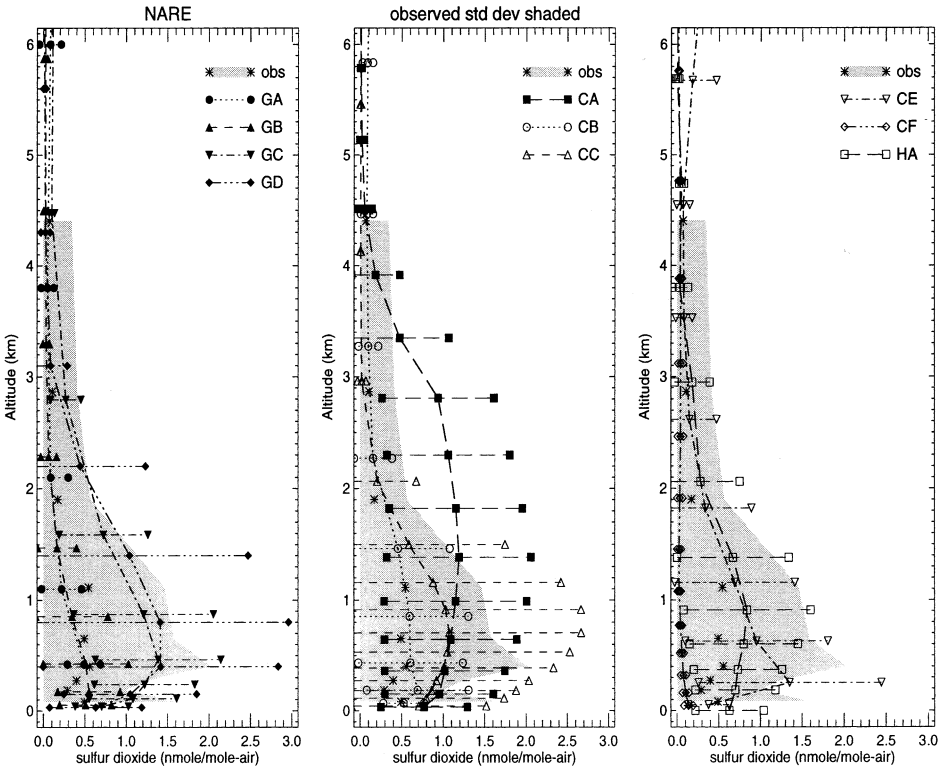


*Fig. 14.* Vertical profile of $SO_2$ (ppbv) $\pm$ one standard deviation obtained during NARE from the different models and observations.

factor two, so that its $SO_2$ contribution is 60% suggesting that sulfate is deposited too quickly in CE. On the other hand the $SO_2$ contribution in CF is only 11%. In this case it is caused by the very low $SO_2$ column burden in CE, which amounts only to 15% of the observed. Simulated $H_2O_2$ with CF matches the observations better than simulated with any other model and the liquid water content agrees well with measurements above the layer closest to the surface, suggesting a too efficient in-cloud oxidation of $SO_2$.

Even though the CTMs and GD should have an advantage in simulating the NARE case study because these models were nudged to observed winds for this period, they do not, on average, perform better than the climate models. The NARE site is a coastal location on the edge of the North American source region where advection is a least as important as local chemical and removal processes. Thus the results suggest that the unnudged GCMs are simulating winds fairly well for the NARE location and time.

### 4.3. *The EMEFSII case study*

The models driven by observed winds simulated the period from July 1993 to June 1994 but not the year 1990 during with EMEPSII took place. Therefore, this comparison can oniy reveal if the models, in a statistical way, are able to capture the much higher $SO_2$ concentrations in this location which is closer to the main $SO_2$ source regions but was also conducted in a different season, which affects the $SO_2$ to total sulfur ratio. As radon observations are not available we limit the comparison to the sulfur cycle at this site.

$H_2O_2$ is lower at EMEFSII than at NARE, because of the different season and also because

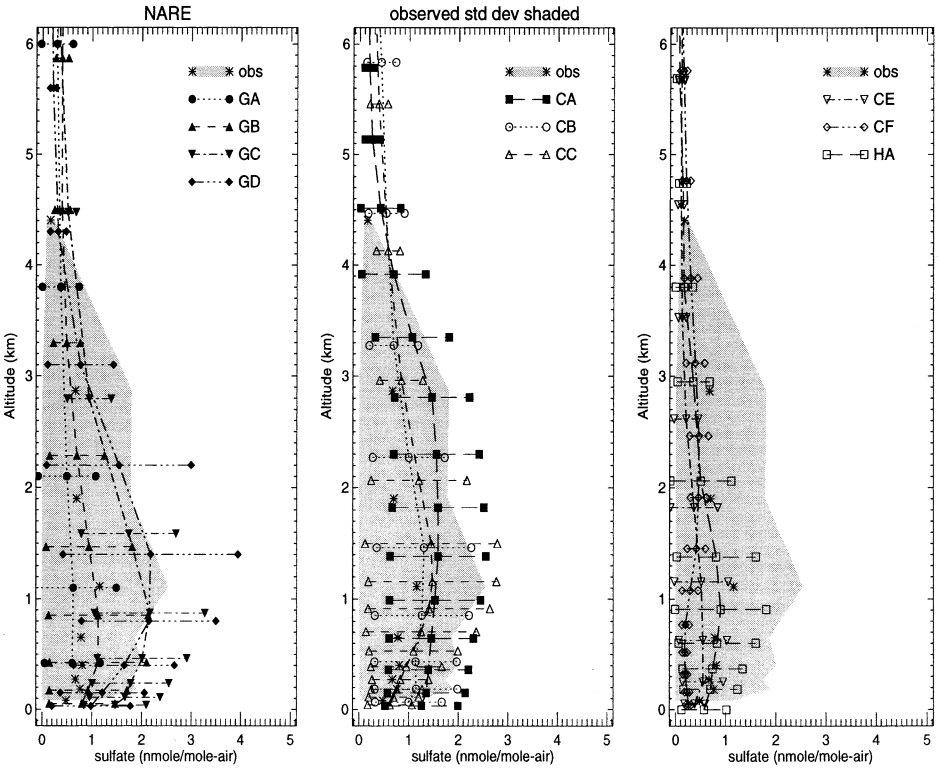


*Fig. 15.* Vertical profile of $SO_4^{2-}$ (ppbv) $\pm$ one standard deviation obtained during NARE from the different models and observations.

Table 6. *Column Burdens at NARE below 3.8 km ($\mu g\ m^{-2}$ of S)*

| | Obs | GA | GB | GC | GD | CA | CB | CC | CE | CF | HA |
|---|---|---|---|---|---|---|---|---|---|---|---|
| $SO_2$ | 1110–1250[a)] | 830 | 780 | 2700 | 2850 | 3920 | 1380 | 1820 | 1930 | 170 | 1840 |
| $SO_4^{2-}$ | 3005–3020 | 2530 | 3390 | 5830 | 6050 | 5770 | 4340 | 4270 | 1460 | 1370 | 2350 |
| $SO_2 + SO_4^{2-}$ | 4130–4255 | 3360 | 4170 | 8530 | 8900 | 9690 | 5720 | 6090 | 3390 | 1540 | 4190 |
| $SO_2/(SO_2 + SO_4^{2-})$ | 0.27–0.29 | 0.25 | 0.19 | 0.32 | 0.32 | 0.40 | 0.24 | 0.30 | 0.57 | 0.11 | 0.44 |

[a)]The range in the observations refers to the 3 and 5 km profiles, respectively.

the region is more polluted. In March/April, the main source of $H_2O_2$, photochemistry, is much weaker than in August/September when the NARE experiment took place. Thus the observed $H_2O_2$ concentrations are below 0.7 ppbv everywhere (Fig. 16). Although some models deviate from the average observed $H_2O_2$ concentrations by more than a factor of two, the modelled standard deviations from all models overlap everywhere with the observed ones. The $O_3$ mixing ratios are comparable to those during NARE (not shown).

The maximum observed LWC is 30 mg kg$^{-1}$ at 2.8 km at Egbert and 12 mg kg$^{-1}$ at 1.9 km for Lake Traverse. As the LWC is highly variable, all models except CA above 1.5 km and CC below 1.2 km are within the standard deviation of the observations. Again CF is the only model to simulate high LWC near the surface (Fig. 17).

Fig. 18 shows vertical profiles of $SO_2$ during

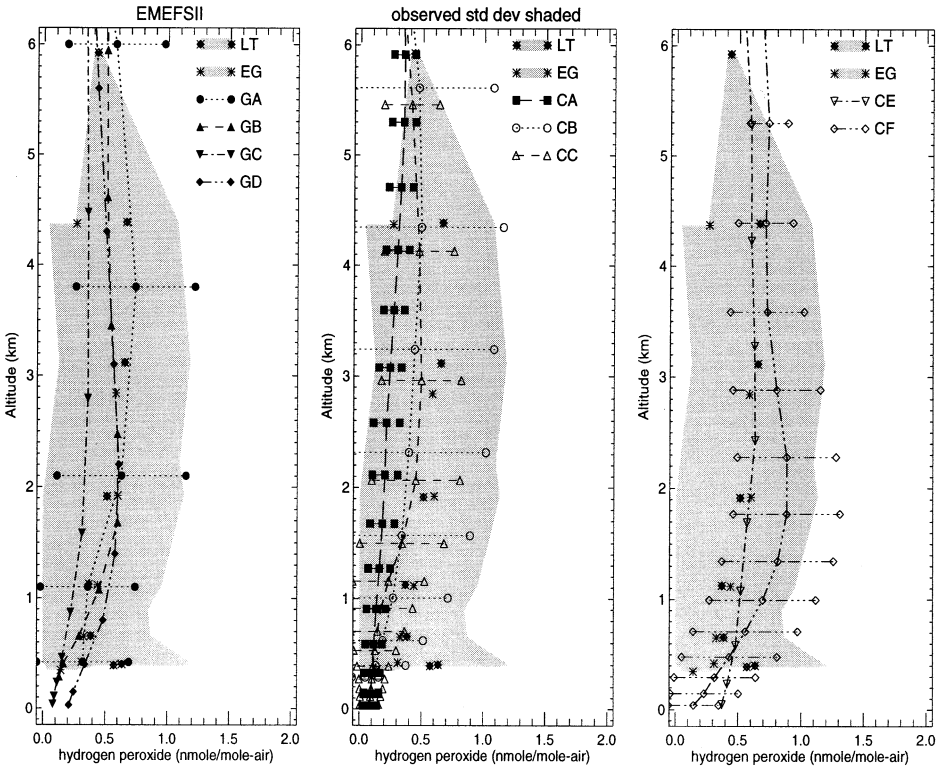


*Fig. 16.* As Fig. 10, but for EMEFSII. LT refers to Lake Traverse and EG to Egbert.

EMEFSII. The observed mixing ratios at Lake Traverse with 1.5 ppbv at 500 m are much lower than at Egbert with 6.5 ppbv at the same altitude, because Egbert is closer to the $SO_2$ source region than Lake Traverse. Between 1 km and 4 km the $SO_2$ mixing ratios at both sites are similar, decreasing from 3–4 ppbv at 1 km to 1 ppbv at 4.5 km. Measurements taken in clear sky only or averaged over cloudy and clear events provide the same averages to within 50%. Most models (8 of 10) simulate $SO_2$ profiles closer to the less polluted profiles of Lake Traverse. The surface mixing ratios vary from 1 to 9.5 ppbv between the models. All models, except CB, underestimate $SO_2$ above the boundary layer. As for NARE, CF simulates low $SO_2$ mixing ratios likely to be caused by a high aqueous phase production rate in the fog (cf. Fig. 17). All models fall within the observed standard deviation. The large value of over 10 ppbv at 6 km originates from the Redoubt volcano in Alaska.

As shown in Fig. 19, $SO_4^{2-}$ mixing ratios are 0.2 ppbv at 6 km and increase to 0.5 ppbv at 600 m in Lake Traverse and 1 ppbv at 300 m at the more polluted site of Egbert. This higher ratio of $SO_2$ to $SO_4^{2-}$ is typical for northern/boreal winter, where less oxidants are available to oxidize $SO_2$. The vertical profiles of sulfate aerosols differ considerably between the models. The low sulfate mixing ratios of 0.2 ppbv above 3 km are captured by half of the models (GB, GD, CE, CF and HA) while they are overestimated outside the observed standard deviation by the rest of the models.

A good agreement can be expected from models, which either calculate the full oxidant chemistry or, at least, solve prognostic equations for $H_2O_2$. Out of that subgroup the two GCMs (GA and GB) enclose the observed $SO_4^{2-}$ mixing ratios in their mean $SO_4^{2-}$ $\pm$ one standard deviation. The GC GCM drastically overestimates $SO_4^{2-}$ above 500 m. It does not solve a prognostic equation for $H_2O_2$ and uses its own winds which may differ strongly from the winds used in the nudged GD

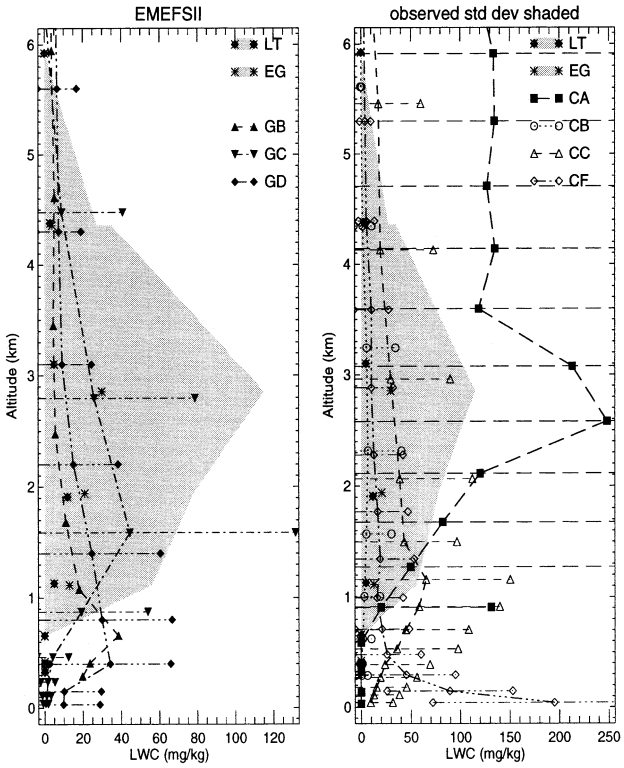


*Fig. 17.* As Fig. 13, but for EMEFSII. LT refers to Lake Traverse and EG to Egbert.

GCM. In addition to that, the $^{222}Rn$ profile of GC suggests a well mixed boundary layer, so that much $SO_2$ and $SO_4^{2-}$ is transported away from the surface before it is deposited.

$SO_4^{2-}$ is also overestimated in the CTMs CA, CB and CC. Of these models, only CB solves prognostic equations for the oxidant chemistry. However, all of them use the same ECMWF winds which the GD GCM is nudged towards, so that differences between large-scale transport are eliminated between them. As their $SO_2$ concentrations are lower than observed, the most likely reason is a too large aqueous phase oxidation rate in all of them, caused by larger than observed liquid water contents in CA and CC and higher than observed ozone mixing ratios in CB.

Table 7 summarizes $SO_2$ and $SO_4^{2-}$ column burdens at EMEFSII. As compared to NARE the total sulfur burden is twice as high in the observations and $SO_2$ contributes to 80% of the column burden, typical for winter–spring. Only two models are able to simulate $SO_2$ contributions of more than 70%, namely those models, which deviate most from the observed $SO_2$ to total sulfur ratio at the NARE site (CE, CF). $SO_2$ contributes only 60% or less in GA, GC and CC. In CC and

Table 7. *Column Burdens at EMEFSII below 3.8 km ($\mu g\ m^{-2}$ of S)*

| | Obs | GA | GB | GC | GD | CA | CB | CC | CE | CF | HA |
|---|---|---|---|---|---|---|---|---|---|---|---|
| $SO_2$ | 6790–7230 | 3840 | 5040 | 5080 | 4120 | 4740 | 7690 | 4960 | 7860 | 2970 | 3960 |
| $SO_4^{2-}$ | 1360–1870 | 3040 | 2230 | 4880 | 2400 | 2730 | 3780 | 3320 | 1420 | 1090 | 1980 |
| $SO_2 + SO_4^{2-}$ | 8150–9100 | 6880 | 7270 | 9960 | 6520 | 7470 | 11470 | 8280 | 9280 | 4060 | 5940 |
| $SO_2/(SO_2 + SO_4^{2-})$ | 0.83–0.79 | 0.56 | 0.69 | 0.51 | 0.63 | 0.63 | 0.67 | 0.6 | 0.85 | 0.73 | 0.67 |

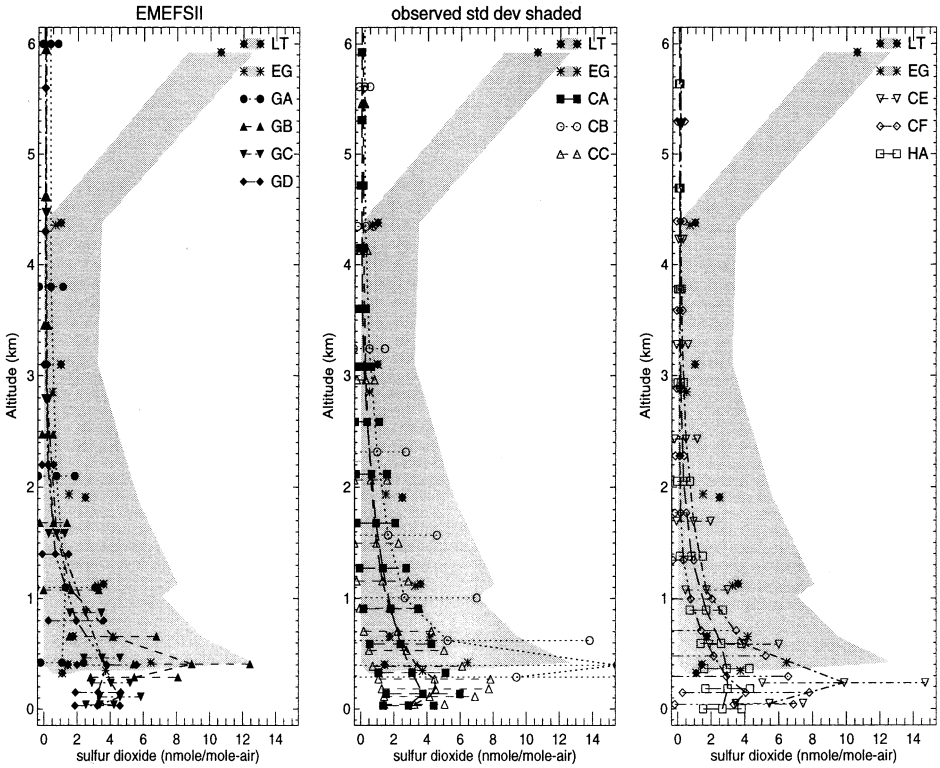


*Fig. 18.* As Fig. 14, but for EMEFSII. LT refers to Lake Traverse and EG to Egbert.

GC it can be attributed to the much higher $SO_4^{2-}$ column burden than observed in combination with a reasonable $SO_2$ column burden. In GA the $SO_2$ burden is underestimated and the $SO_4^{2-}$ burden overestimated. A plausible explanation for GC and CC's high sulfate burden is a rather high liquid water content as compared with observations which could have caused more aqueous phase sulfate production than observed. If these clouds did not precipitate as much or as frequently as observed than these clouds would only provide a source for $SO_4^{2-}$ but not a sink. As precipitation or wet deposition are not available from the observations a more quantitative assessment is beyond the scope of this study.

## 5. Conclusions

Vertical profiles of $SO_2$ and $SO_4^{2-}$ from ten models have been compared with observations at two locations in North America. Additionally, pole-to-pole meridional transects of $SO_2$ and $SO_4^{2-}$ were compared between different models along 80°W. There are two peaks in $SO_2$ along the transect in DJF: one at 30–60°N associated with the eastern North American source region and one in the Arctic associated with long range transport of $SO_2$ to the Arctic from Eurasia which are captured by HA, GC and GD. In JJA only the peak over eastern North America is evident in all models while no peak appears in the Arctic.

While no single model stands out as being best or worst as compared to observations during NARE and EMEFSII, the general tendency is that those models simulating the full oxidant chemistry tend to agree better with observations. That is, none of the models running with full chemistry deviates more than a factor of two from the observed $SO_2$ or $SO_4^{2-}$ column burdens or from the observed ratio of $SO_2$ to total sulfur at the EMEFSII and NARE sites. On the other hand the models outside a factor of two from the observations solve at most prognostic equations

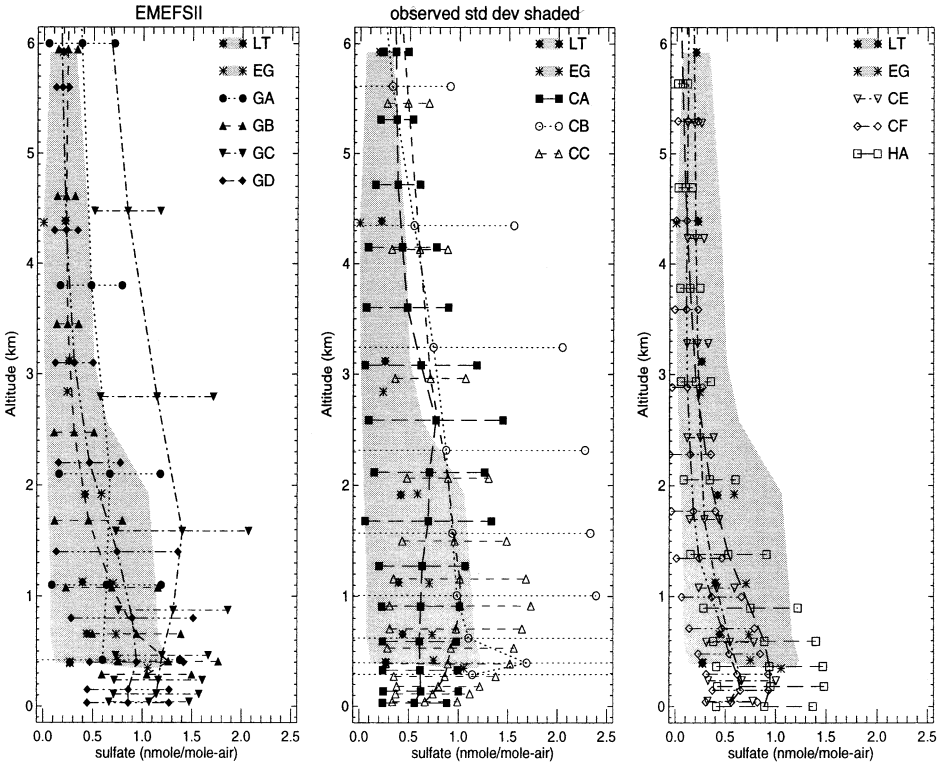


*Fig. 19.* As Fig. 15, but for EMEFSII. LT refers to Lake Traverse and EG to Egbert.

for $H_2O_2$ and OH but in most cases import monthly mean three-dimensional mixing ratios of at least one oxidant. Similar conclusions were drawn by Roelofs et al. (1998) who compared the simulated sulfur cycle using calculated and prescribed oxidant fields.

Comparing the vertical profiles of $SO_2$ and sulfate aerosols at EMEFSII from a simulation with a prognostic equation for $H_2O_2$ as done in the climate model GA and one without as in the climate model GC suggests the need for a prognostic equation for $H_2O_2$. In GC the $SO_2$ mixing ratios were almost completely depleted in the free atmosphere and $SO_4^{2-}$ overestimated as compared to observations. This effect is not as strong in GA, where $H_2O_2$ is depleted by the oxidation with $SO_2$ in the aqueous phase by solving a prognostic equation for $H_2O_2$. However, this conclusion does not extend to the chemical transport models. Only the models CA and CE use prescribed oxidant fields and their simulated $SO_2$ mixing ratios at EMEFSII are similar to those of the other transport models. More importantly, the simulated $SO_4^{2-}$ mixing ratios of CE are lower and in better agreement with observations than those simulated with CB, CC or CF.

Clearly the comparison with observations taken at only two measurement sites is not enough. One problem in the comparison arises from the uncertainties associated with comparing essentially point observations with model averages for grids that are 200–500 km across. Another problem with the NARE case study in particular is its location at the coast where the observed trace gas mixing ratios have not only local sources due to DMS oxidation, but are strongly influenced by advection. The advective $SO_2$ and $SO_4^{2-}$ mixing ratios depend strongly on the prevailing wind direction, such that south-westerly winds bring polluted air to the NARE site while northerly winds bring remote air to the NARE site. Moreover, the results at the NARE site depend on the land-sea mask of the individual models as well as on the horizontal resolution. Thus, many

more measurements of vertical profiles of $SO_2$, $SO_4^{2-}$, liquid water content and oxidant mixing ratios are needed for a more quantitative comparison with model simulations.

## 6. Acknowledgments

We thank 2 anonymous reviewers for helpful comments and suggestions. We are grateful to Ms. Nicole Schantz of MSC for processing the NARE and EMEFSII profile data and to Larry Kleinman of Brookhaven National Laboratory for providing the NARE $H_2O_2$ data. We thank WCRP for support.

REFERENCES

Banic, C. M., Leaitch, W. R., Isaac, G., Couture, M. D., Kleinman, L. I., Springston, S. R. and MacPherson, J. I. 1996. Transport of ozone and sulfur to the North Atlantic atmosphere during the North Atlantic Regional Experiment. *J. Geophys. Res.* **101**, 29,091–29,104.

Barrie, L., Yi, Y., Lohmann, U., Leaitch, W. R., Kasibhatla, P., Roelofs, G.-J., Wilson, J., McGovern, F., Benkovitz, C., Meliere, M. A., Law, K., Prospero, J., Kritz, M., Bergmann, D., Bridgeman, C., Chin, M., Christensen, J., Easter, R., Feichter, J., Jeuken, A., Kjellström, E., Koch, D., Land, C. and Rasch, P. 2001. A comparison of large scale atmospheric sulphate aerosol models (COSAM): overview and highlights. *Tellus* **53B**, this issue.

Barrie, L. A. 1996. *Chemical exchange between the atmosphere and polar snow*. NATO ASI Series I: Global environmental change, vol. 43, ch. Occurrence and trends of pollution in the Arctic troposphere, pp. 93–130.

Barth, M. C., Rasch, P. J., Kiehl, J. T., Benkovitz, C. M. and Schwartz, S. E. 2000. Sulfur chemistry in the National Center for Atmospheric Research Community Climate Model: description, evaluation, features, and sensitivity to aqueous chemistry. *J. Geophys. Res.* **105**, 1387–1415.

Berge, E. 1993. Coupling of wet scavenging of sulphur to clouds in a numerical weather prediction model. *Tellus* **45B**, 1–22.

Chin, M., Jacob, D. J., Gardner, G. M., Foreman-Fowler, M. S. and Spiro, P. A. 1996. A global three-dimensional model of tropospheric sulfate. *J. Geophys. Res.* **101**, 3761–3778.

Chin, M., Rood, R. B., Lin, S.-J., Müller, J.-F. and Thompson, A. M. 2000. Atmospheric sulfur cycle simulated in the global model GOCART: model description and global properties. *J. Geophys. Res.* **105**, 24,671–24,688.

Christensen, J. H. 1997. The danish eulerian hemispheric model — a three-dimensional air pollution model used for the arctic. *Atmos. Environ.* **31**, 4169–4191.

Dentener, F., Feichter, J. and Jeuken, A. 1999. Simulation of the transport of $^{222}Rn$ using on-line and off-line global models at different horizontal resolutions: a detailed comparison with measurements. *Tellus* **51B**, 573–602.

Fehsenfeld, F. C., Daum, P., Leaitch, W. R., Trainer, M., Parrish, D. D. and Huebler, G. 1996. Transport and processing of $O_3$ and $O_3$ precursors over the North Atlantic: an overview. *J. Geophys. Res.* **101**, 28,877–28,891.

Feichter, J., Kjellström, E., Rodhe, H., Dentener, F., Lelieveld, J. and Roelofs, G.-J. 1996. Simulation of the tropospheric sulfur cycle in a global climate model. *Atmos. Environ.* **30**, 1693–1707.

Feichter, J. and Lohmann, U. 1999. Can relaxation technique be used to validate clouds and sulphur species in a GCM? *Q. J. R. Meteorol. Soc.* **125**, 1277–1294.

Ganzeveld, L., Lelieveld, J. and Roelofs, G.-J. 1998. A dry deposition parameterization for sulfur oxides in a chemistry and general circulation model. *J. Geophys. Res.* **103**, 5679–5694.

Giannakopoulos, C., Chipperfield, M. P., Law, K. S. and Pyle, J. A. 1999. Validation and intercomparison of wet and dry deposition schemes using $^{210}Pb$ in a global three-dimensional off-line chemical transport model. *J. Geophys. Res.* **104**, 23,761–23,784.

Giorgi, F. and Chameides, W. L. 1986. Rainout lifetimes of highly soluble aerosols and gases inferred from simulations with a general circulation model. *J. Geophys. Res.* **91**, 14,367–14,376.

Issac, G. A., Banic, C. M., Leaitch, W. R., Anlauf, K. G., Couture, M. D., Liu, P. S. K., Macdonald, A. M., MacQuarrie, K. I. A., Puckett, K. J. and Wiebe, H. A. 1998. Vertical profiles and horizontal transport of atmospheric aerosols and trace gases over central Ontario. *J. Geophys. Res.* **103**, 22,015–22,037.

Jacob, D. J., Prather, M. J., Rasch, P. J., Shia, R.-L., Balkanski, Y. J., Beagley, S. R., Bergmann, D. J., Blackshear, W. T., Brown, M., Chiba, M., Chipperfield, M. P., Grandpre, J. D., Dignon, J. E., Feichter, J., Genthon, C., Grose, W. L., Kasibhatla, P. S., Koehler, I., Kritz, M. A., Law, K., Penner, J. E., Ramonet, M., Reeves, C. E., Rotman, D. A., Stockwell, D. Z.,

Velthoven, P. F. J. V., Verver, G., Wild, O., Yang, H. and Zimmermann, P. 1997. Evaluation and intercomparison of global atmospheric transport models using $^{222}$Rn and other short-lived tracers. *J. Geophys. Res.* **102**, 5953–5970.

Jeuken, A. B. M., Siegmund, P. C., Heijboer, L. C., Feichter, J. and Bengtsson, L. 1996. On the potential of assimilating meteorological analyses in a global climate model for the purpose of model validation. *J. Geophys. Res.* **101**, 16,939–16,950.

Koch, D. M., Jacob, D. J., Rind, D., Chin, M. and Tegen, I. 1999. Tropospheric sulfur simulation and sulfate direct radiative forcing in the Goddard Institute for Space Studies general circulation model. *J. Geophys. Res.* **104**, 23,799–23,822.

Law, K. S., Plantevin, P.-H., Shallcross, D. E., Rogers, H., Grouhel, C., Thouret, V., Marenco, A. and Pyle, J. A. 1998. Evaluation of modelled $O_3$ using mozaic data. *J. Geophys. Res.* **103**, 25,721–25,740.

Lohmann, U., Von Salzen, K., McFarlane, N., Leighton, H. G. and Feichter, J. 1999. The tropospheric sulfur cycle in the Canadian general circulation model. *J. Geophys. Res.* **104**, 26,833–26,858.

Merrill, J. T. and Moody, J. L. 1996. Synoptic meteorology and transport during the North Atlantic Regional Experiment (NARE) intensive. *J. Geophys. Res.* **101**, 28,903–28,921.

Muller, J. F. and Brasseur, G. 1995. IMAGES — a 3 dimensional chemical transport model the global troposphere. *J. Geophys. Res.* **100**, 16,445–16,490.

Penner, J. E., Bergmann, D., Walton, J. J., Kinnison, D., Prather, M. J., Rotman, D., Price, C., Pickering, K. E. and Baughcum, S.-L. 1998. An evaluation of upper tropospheric $NO_x$ with two models. *J. Geophys. Res.* **103**, 22,097–22,113.

Pham, M., Mueller, J.-F., Brasseur, G. P., Granier, C. and Megie, G. 1995. A three-dimensional study of the tropospheric sulfur cycle. *J. Geophys. Res.* **100**, 26,061–26,092.

Rasch, P. J., Feichter, J., Law, K., Mahowald, N., Penner, J. et al., 2000. A comparison of scavenging and deposition processes in global models: results from WCRP Cambridge Workshop of 1995. *Tellus* **52B**, 1025–1056.

Rasch, P. J., Mahowald, N. M. and Eaton, B. E. 1997. Representations of transport, convection, and the hydrologic cycle in chemical transport models: implications for the modeling of short-lived and soluble species. *J. Geophys. Res.* **102**, 28,127–28,138.

Roelofs, G.-J., Kasibhatla, P., Barrie, L., Bergmann, D., Bridgeman, C., Chin, M., Christensen, J., Easter, R., Feichter, J., Jeuken, A., Kjellström, E., Koch, D., Land, C., Lohmann, U., Rasch, P. and Yi, Y. 2001. Analysis of regional budgets of sulfur species modelled for the COSAM exercise. *Tellus* **53B**, this issue.

Roelofs, G.-J., Lelieveld, J. and van Dorland, R. 1998. Simulation of global sulfate distribution and the influence on effective cloud drop radii with a coupled photochemistry-sulfur cycle model. *Tellus* **50B**, 224–242.

Saylor, R. D., Easter, R. C. and Chapman, E. G. 1999. Simulation of the tropospheric distribution of carbon monoxide during the 1984 MAPS experiment. *Atmos. Environ.* **33**, 4675–4694.

Voldner, E. C., Barrie, L. A. and Sirois, A. 1986. A literature review of dry deposition of oxides of sulphur and nitrogen with emphasis on long-range transport modelling in North America. *Atmos. Env.* **20**, 2101–2123.

Weinstien-Lloyd, J. B., Daum, P. H., Nunnermacker, L. J., Lee, J. H. and Kleinman, L. I. 1996. Measurement of peroxides and related species in the 1993 North Atlantic Regional Experiment. *J. Geophys. Res.* **101**, 29,081–29,090.

Wesely, M. L. and Hicks, B. B. 1977. Some factors that affect the deposition rates of sulfur dioxide and similar gases on vegetation. *J. Air Pollut. Contr. Assoc.* **27**, 1110–1116.

Zaucker, F., Daum, P. H., Wetterauer, U., Berkowitz, C., Kromer, B. and Broecker, W. S. 1996. Atmospheric $^{222}$Rn measurements during the 1993 NARE intensive. *J. Geophys. Res.* **101**, 29,149–29,164.